Theoret. Comput. Fluid Dynamics (2001) 14: 293–322

Theoretical and Computational Fluid Dynamics

Equilibrium Statistical Predictions for Baroclinic Vortices: The Role of Angular Momentum

Mark T. DiBattista⋆ and Andrew J. Majda⋆⋆

Courant Institute of Mathematical Sciences, New York University,
251 Mercer Street, New York, NY 10012, U.S.A.

Communicated by H.J.S. Fernando

Received 12 April 2000 and accepted 21 September 2000

Abstract. We develop a point-vortex equilibrium statistical model for baroclinic quasigeostrophic vortices within the context of a two-layer quasigeostrophic fluid that evolves in all of space. Angular momentum, which follows from the rotational symmetry of the unbounded domain, is the key conserved quantity, introducing a length scale that confines the most probable states of the statistical theory. We apply the theory as a model of localized convection in a preconditioned gyre. To illustrate this application, the preconditioned cyclonic, largely barotropic gyres are modeled as "zero inverse temperature" states, which are explicit solutions to the mean-field equations with a Gaussian probability distribution of vortices. Convection is modeled by a cloud of point-vortex hetons – purely baroclinic arrangements of point vortices, cyclonic above and anticyclonic below – which capture the short-term, geostrophically balanced response to strong surface cooling. Numerical heton studies (Legg and Marshall, 1993, 1998) have shown that a preexisting barotropic rim current can suppress baroclinic instability and confine anomalies of potential vorticity and temperature introduced by the cold-air outbreak. Here, we demonstrate that the lateral extent of the most probable states of the statistical theory are constrained by the angular momentum. Without resolution of the detailed dynamics, the equilibrium statistical theory predicts that baroclinic instability is suppressed for preconditioned flows with potential vorticity of the same sign in each layer provided that the strength of convective overturning does not change the sign of potential vorticity in one of the layers. This result agrees with detailed simulations (Legg and Marshall, 1998) and supports the potential use of these statistical theories as parametrizations for crude closure.

1. Introduction

Equilibrium statistical theory is an attractive model for a wide range of atmospheric and oceanographic phenomena, producing large-scale, steady coherent structures as the statistically most probable endstate of an evolving fluid. Equilibrium statistical models have been proposed for oceanic basin flow dominated by bottom topography (Salmon *et al.*, 1976; Carnevale and Frederiksen, 1987; Grote and Majda, 2000), Jupiter's Great Red Spot (Miller *et al.*, 1992), and as closure parameters in barotropic ocean models (Grote and Majda, 1997; Kazantsev *et al.*, 1998; DiBattista and Majda, 1999b).

The authors have developed an equilibrium statistical theory for open-ocean deep convection, which, in bounded domains, models the effects of statistically homogeneous surface cooling over quiescent initial flow

⋆ Mark DiBattista was supported as a post-doctoral fellow at the Courant Institute through NSF DMS-9625795.

⋆⋆ Andrew Majda's research was partially supported by Grants NSF DMS-9972865, NSF DMS-9625795, ONR N00014-96-1-0043, and ARO DAAG55-98-1-0129.

(DiBattista and Majda, 1999a, 2000) and flow preconditioned by topography and surface-wind stress (DiBattista *et al.*, 2000). In this paper, in contrast, the fluid evolves in all of space so that rotational symmetry introduces an additional constraint on the angular momentum in the flow. This is a useful model for *localized* convective overturning induced by localized cooling within preconditioned ocean sites with very distant boundaries and we find that commonly observed features in simple numerical models – such as the suppression of baroclinic instability by a dominant barotropic governor (James, 1987; Legg and Marshall, 1998) – are present in the most probable states predicted by the equilibrium theory. The qualitative and quantitative agreement of the statistical theory presented here with facets of earlier numerical simulations supports the potential use of these statistical theories as parametrizations in closure modeling.

More specifically, we have tailored a point-vortex equilibrium statistical theory for the two-layer quasigeostrophic fluid model that predicts the spread of cold-temperature and vorticity anomalies introduced by localized cooling in the open ocean. The two-layer model, which is discussed in Section 2.1, consists of a coupled pair of two-dimensional fluids, in which pressure variations in one layer excite horizontal motion in the other layer. The two-layer quasigeostrophic model can be decomposed into two independent parts, a barotropic component that measures the portion of the flow that is common to both layers and a baroclinic component that governs motion induced by pressure differences between the two layers. The statistical theory is summarized in Section 3 of this paper but a detailed formal derivation of the statistical theory is relegated to the Appendix since it parallels earlier derivations for barotropic flow (Caglioti *et. al.*, 1992; Kiessling, 1993).

Convective overturning, which occurs in waters at extreme polar latitudes such as the Labrador Sea, Greenland Sea, and the Weddell Sea as well as in the Mediterranean Sea, is driven by extreme differences in temperature between the relatively warm ocean and the cold atmosphere above. In DiBattista and Majda (1999a, 2000) and DiBattista *et. al.* (2000) the fluid domain is contained within a closed basin and the convective forcing appears most naturally in the statistical theory as spread homogeneously across the domain.

Numerical simulations of convective overturning, however, have modeled *localized* surface cooling (Legg and Marshall, 1993, 1998; Legg *et. al.*, 1996) using simplified point-vortex models for convective towers called "hetons" (Hogg and Stommel, 1985). These studies demonstrate the stabilizing properties of the barotropic governor. In particular, the "products" of convection – the cold-temperature and vorticity anomalies due to the loss of buoyancy in the ocean interior – are confined to the center of the gyre, which strongly suppresses any escape by means of baroclinic instability (Legg and Marshall, 1993, 1998). The introduction of hetons as models for convective overturning motivates our choice of a point-vortex equilibrium statistical theory. The earlier idealized theory (DiBattista and Majda, 1999a, 2000; DiBattista *et. al.*, 2000) with basin-wide cold-air outbreaks from land masses inducing convection is most natural for the polar oceans. The statistical model for the response to localized cooling that is the main focus of this paper is more appropriate as a model for the open-ocean convection site at the Gulf of Lions in the Mediterranean. There, localized cooling and preconditioned localized wind-driven gyres are generated by mistral winds from the Rhone valley (Marshall and Schott, 1999). Localized disk cooling is also prominent in laboratory experiments on rotating convection (Marshall and Schott, 1999).

In this paper an equilibrium statistical model for localized convective forcing is accomplished by what may initially appear to be an unlikely means: we change the domain of the fluid from a closed basin to all of space. The key property of the unbounded domain is rotational symmetry, which introduces an additional, and quite powerful, constraint on the angular momentum of the total flow. The angular momentum constraint introduces a length scale, L_A, that confines the most probable states, thus capturing the effects of "boundedness" of flow in the infinite plane. The length scale L_A is the typical radius of the vortex formed from the barotropic component of the potential vorticity field. The elementary exact solutions in Section 4 establish a clear link between this length scale and angular momentum. With respect to models for open-ocean convection, the angular momentum constrains both the preexisting cyclonic flow in preconditioned convection sites and the distribution of convective forcing, which contains no angular momentum of its own. Furthermore, as discussed in the Appendix, confinement of the most probable states requires that the potential vorticity be of a single sign in both layers, which prevents the formation of vortex clumps of opposite sign. There are rigorous theorems (Lim and Majda, 2000) demonstrating that such an equilibrium statistical theory is impossible for vorticity of opposite sign in each layer because there are tilted dipole clusters, with positive measure in phase space, that propagate outside any bounded region. Such behavior is an important facet of heton dynamics in a quiescent unbounded domain (Legg and Marshall, 1993).

There is an additional length scale, L_ρ, known as the Rossby radius of deformation, that is derived from the coupling strength of the upper and lowers layers of the fluid. This length scale measures the influence of the baroclinic field, and in oceanographic contexts is usually much smaller in extent that the width of the dominant vortical flow, i.e., $L_A \gg L_\rho$. In this regime the influence of the baroclinic component of the flow is much less than the typical spread of the upper and lower vortices. The nonvanishing baroclinic component of the flow introduces novel elements into the point-vortex statistical theory.

The outline for this paper is as follows. We introduce the two-layer quasigeostrophic model over all of space in Section 2, defining the conserved quantities, energy, circulation, and angular momentum for an unbounded fluid. In Section 3 we develop the equilibrium statistical theory for a small-scale potential vorticity field parametrized by both point vortices of fixed strength and by a uniform measure over a finite interval. The key tool of the statistical theory is a coupled pair of nonlinear elliptic partial differential equations – called the *mean-field equations* – whose solution yields the most probable state of the mean vorticity field. In Section 4 we explore a special parameter regime in which the mean-field equations are linear, with explicit solutions that take a simple Gaussian form. The application of the equilibrium statistical model is developed in Sections 5 and 6, first as models for the preconditioned ocean sites, next as models for full-fledged open-ocean convection.

2. Two-Layer Quasigeostrophic Equations and Conserved Quantities for All of Space

The simplest appropriate model is a two-layer quasigeostrophic fluid in which the stratified ocean is partitioned into two thin slabs, each of constant depth, density and temperature. The dynamics of the quasigeostrophic model is governed by the material conservation of "potential vorticity," defined in (2.1), which is a measure of intrinsic vorticity in fluid parcels that undergo changes in ambient conditions of pressure or temperature. Convection is therefore modeled as localized anomalies in the potential vorticity field of the upper and lower layer, a procedure that is described in greater detail in Section 5.1.

The quasigeostrophic fluid treated here evolves in the unbounded infinite plane, which supports a set of quantities that are conserved under the flow, such as the pseudoenergy, angular momentum, and circulation in the upper and lower layers. These quantities serve as the basis of the equilibrium statistical theory developed in Section 3. We also present the typical length and time scales that serve to nondimensionalize the problem.

2.1. Two-Layer Quasigeostrophic Fluid Model

We develop the equilibrium statistical theory within the context of a stably stratified, two-layer quasigeostrophic model. In this model the fluid is composed of two thin layers of equal depth, each of constant density and temperature, bound by flat surfaces on the top and bottom. Within each layer there is no vertical shear in the velocity field, so that the flow is essentially two-dimensional. The potential vorticity in the upper and lower layers, q_1 and q_2, and the stream functions in the upper and lower layers, ψ_1 and ψ_2, are coupled through the relations

$$\begin{aligned} q_1 &= \Delta\psi_1 - F(\psi_1 - \psi_2), \\ q_2 &= \Delta\psi_2 + F(\psi_1 - \psi_2), \end{aligned} \tag{2.1}$$

where F is the "rotational Froude number" (Pedlosky, 1979). In (2.1), Δ denotes the horizontal Laplacian. From (2.1) F has units, length^{-2}, so that $F = L_\rho^{-2}$, with L_ρ the Rossby radius of deformation – the scale at which horizontal pressure differences can induce vertical shear, i.e., differences between the upper and lower layer in the velocity field. In this paper we use a nondimensional length scale defined by the Rossby radius, L_ρ; thus, we fix the deformation radius to be unity, i.e., $F = 1$. The fluid evolves within an unbounded domain that extends through all of space. With these nondimensionalizations, the pressure in each layer is given by the stream function.

The potential vorticities q_1 and q_2 in (2.1) are each materially conserved in the quasigeostrophic model, so that

$$\begin{aligned} \frac{\partial q_1}{\partial t} + \nabla^\perp \psi_1 \cdot \nabla q_1 &= 0, \\ \frac{\partial q_2}{\partial t} + \nabla^\perp \psi_2 \cdot \nabla q_2 &= 0, \end{aligned} \tag{2.2}$$

where the symbol $\nabla^\perp \equiv \hat{k} \times \nabla$ is the perpendicular gradient operator. Together with the conditions of vanishing flow at infinity,

$$\nabla \psi(x) \to 0 \qquad \text{as} \quad |\boldsymbol{x}| \to \infty, \tag{2.3}$$

the evolution of the two-layer fluid is completely determined by the initial values of the potential vorticities, q_1 and q_2, in (2.1).

It is useful to decompose the potential vorticity fields, q_1 and q_2, and the stream functions, ψ_1 and ψ_2, into two independent, physically meaningful components:

$$\begin{aligned} \psi_{\mathrm{B}} &= \frac{\psi_1 + \psi_2}{2}, \qquad & q_{\mathrm{B}} &= \frac{q_1 + q_2}{2}, \\ \psi_{\mathrm{T}} &= \frac{\psi_1 - \psi_2}{2}, \qquad & q_{\mathrm{T}} &= \frac{q_1 - q_2}{2}. \end{aligned} \tag{2.4}$$

The barotropic components, which are designated by a subscript B, contain the portion of the flow that is common to both upper and lower layers, and thus describes the flow that is independent of deformations of the fluid interface. The baroclinic components, which are designated by a subscript T, arise from horizontal pressure differences in the flow that are due to undulations in the interface that separates the upper and lower layers. Vertical shears, which are differences between the two layers, are therefore induced by the baroclinic components of the flow.

The barotropic and baroclinic components of the potential vorticity and stream function fields are related by

$$\Delta \psi_{\mathrm{B}} = q_{\mathrm{B}}, \tag{2.5}$$

$$\Delta \psi_{\mathrm{T}} - 2F\psi_{\mathrm{T}} = q_{\mathrm{T}}, \tag{2.6}$$

which is derived by inverting the upper- and lower-layer potential vorticities and stream functions in (2.4) and substituting back into the potential vorticity-stream function relations in (2.1). The stream functions induced by barotropic and baroclinic arrangements of point vortices in the potential vorticity field are given by Green's functions, G_{B} and G_{T}, which are the kernels of the integral operators that invert the relations in (2.5) and (2.6), respectively:

$$G_{\mathrm{B}}(\boldsymbol{x}_1, x_2) = \frac{1}{2\pi} \ln |\boldsymbol{x}_1 - x_2| \,, \tag{2.7}$$

$$G_{\mathrm{T}}(\boldsymbol{x}_1, x_2) = -\frac{1}{2\pi} K_0 \left(\sqrt{2F} |\boldsymbol{x}_1 - x_2| \right). \tag{2.8}$$

The influence of the barotropic fields, given by G_{B}, is long in range and controls the falloff in the velocity field at large distances. The influence of the baroclinic fields, given by G_{T}, is short in range, since K_0, which is a modified Bessel function of the first kind, effectively vanishes at distances greater than $1/\sqrt{F}$. We exploit the properties of Green's functions, G_{B} and G_{T}, in the numerical algorithm developed in Section 4.3 that produces the most probable states of the statistical theory.

Since the quasigeostrophic model given in (2.1) is stably stratified, the lower layer contains fluid that is denser and cooler than the upper layer. Therefore, the position of the fluid interface – whether it lies above or below the position of the flat undisturbed state – indicates the relative temperature in a column of fluid. Furthermore, it is possible to define the relative temperature of a fluid column in terms of the baroclinic stream function, ψ_{T}, and the coupling parameter, F (Pedlosky, 1979):

$$\text{deformation of fluid interface} = -F\psi_{\mathrm{T}}. \tag{2.9}$$

A region in which the interface domes upward contains a greater proportion of colder fluid in the lower layer to warmer fluid in the upper layer and so is relatively cold; similarly, a depression of the interface yields a fluid column that is relatively warm. In the contexts of Sections 5 and 6, where we develop an equilibrium statistical theory for convective overturning in the open ocean, the position of the interface separating the upper and lower layers of a preconditioned initial state is referred to as the "preconditioned thermal field" and any additional change of the interface following convective overturning as a "temperature anomaly."

2.2. Conserved Quantities in the Two-Layer Quasigeostrophic Model

There are two types of quantities that are conserved in the two-layer quasigeostrophic model: (1) those that follow from symmetries of time and space and (2) those that follow from the dynamic condition in which potential vorticity is simply advected by the flow.

Since the infinite plane is invariant under both linear displacements and rotations, both the center of vorticity, $\boldsymbol{M}$, and angular momentum, A, are conserved under the evolution of the flow in (2.2); the pseudoenergy, H, is also conserved and follows from symmetry in time.

Conserved Quantities.

$$\begin{aligned} H &= \sum_{j=1}^{2} -\frac{1}{2}\int_{\mathcal{R}^2} \psi_j q_j, \\ \boldsymbol{M} &= \sum_{j=1}^{2} \int_{\mathcal{R}^2} q_j \boldsymbol{x}, \\ A &= \sum_{j=1}^{2} \int_{\mathcal{R}^2} q_j |\boldsymbol{x}^2|. \end{aligned} \tag{2.10}$$

In the quasigeostrophic fluid model the potential vorticity in (2.2) is materially conserved. Therefore all functions of the potential vorticity are also conserved, which leads to an infinite collection of potential constraints on the flow. However, the small-scale potential vorticity field is approximated in the equilibrium statistical theory, which is developed in the Appendix, by distributions of point vortices. This choice implies that all of the constraints on the small-scale potential vorticity field are inactive, except for the potential circulation, Γ_1 and Γ_2, in each layer:

$$\begin{aligned} \Gamma_1 &= \int q_1, \\ \Gamma_2 &= \int q_2. \end{aligned} \tag{2.11}$$

In the remainder of the paper the terminology circulation is utilized often for the quantities in (2.11). Thus the equilibrium statistical theory is based on the conserved quantities in (2.10) and (2.11). It is important to mention here that the pseudoenergy, H, in (2.10), is not necessarily equivalent to the total standard energy of the flow. In fact, the kinetic energy is infinite due to the slow, $1/r$, decay of the gradient of the barotropic stream function in (2.7) provided that the sum of the circulations in (2.11) is nonzero. The pseudoenergy is a renormalized version of the total energy and is not necessarily positive (Majda and Bertozzi, 2000).

2.3. Nondimensionalization of Length and Time Scales

We anticipate that the typical spread and strength of the most probable solutions predicted by the equilibrium statistical theory are governed by the large-scale conserved quantities defined in (2.10) and (2.11). On the basis of these typical scalings we can set one length parameter, which we choose to be the extent of influence of the baroclinic field defined by the Rossby radius L_ρ discussed earlier, and one time parameter, which we choose to be the rotation time of the barotropic vortex, to unity. These quantities are used to nondimensionalize the length and time scales in the problem.

We claim that the angular momentum, defined in (2.10), is the key quantity that restricts the potential vorticity into confined vortices about the origin. The angular momentum may be rewritten as

$$\begin{aligned} A &= \sum_{j=1}^{2} \int_{\mathcal{R}^2} q_j |\boldsymbol{x}^2| = \int_{\mathcal{R}^2} (q_1 + q_2) |\boldsymbol{x}^2| \\ &= 2 \int_{\mathcal{R}^2} q_{\mathrm{B}} |\boldsymbol{x}^2|, \end{aligned} \tag{2.12}$$

where the barotropic component of the potential vorticity is defined in (2.4). Since angular momentum and circulation have units,

$$[A] \sim L^4 T^{-1}, \qquad [\Gamma] \sim L^2 T^{-1}, \tag{2.13}$$

we can define a large-scale length parameter, L_A, from a combination of these parameters,

$$L_A \sim \sqrt{\frac{A}{2\Gamma_{\mathrm{B}}}}, \tag{2.14}$$

where the form of the angular momentum in (2.12) motivates our use of the circulation in the barotropic field, $\Gamma_{\mathrm{B}} = (\Gamma_1 + \Gamma_2)/2$, to define L_A. The length scale, L_A, is the typical radius of the vortex formed from the barotropic component of the potential vorticity field. Furthermore, the finite-dimensional Gibbs ensembles of point vortices from (A.7) which are utilized in the derivation of the equilibrium statistical theory discussed in the Appendix are finite only if the potential vorticity in both layers is either all positive or all negative, so the barotropic component of the potential vorticity always accounts for more than half of the flow. With two different signs of vorticity, there is exponential growth of the integrand in (A.8) so that $Z(N) = +\infty$ and the Gibbs measure is infinite. Thus, we assume that Γ_{B} is positive in (2.14) and the remainder of the paper without loss of generality.

A second length scale is introduced by Green's function, G_{T} in (2.8), which governs the deformation of the fluid interface separating the upper and lower layers. As mentioned earlier, (2.1), this length scale, L_ρ, is the Rossby radius of deformation. The deformation radius is related to the coupling parameter, F, that measures the "stiffness" of the interface that separates the upper and lower layers,

$$L_\rho \sim \frac{1}{\sqrt{F}}. \tag{2.15}$$

Whereas L_A measures the lateral extent of the potential vorticity field, L_ρ delimits the baroclinic stream function. As mentioned earlier, (2.1), in this paper we set the coupling parameter to unity, i.e., $F = 1$, and use the deformation radius, L_ρ, as the basis for nondimensionalization.

The time scales in the two-layer fluid can be expressed in terms of two quantities: the turnaround time of the barotropic field and a "baroclinicity" parameter that measures the difference in rotation between the upper and lower layers. Since the lateral extent of the barotropic vortex is given by L_A, the turnaround time, which is derived from the units of circulation provided in (2.13), is given by

$$T_{\mathrm{B}} \sim \frac{4\pi L_A^2}{\Gamma_{\mathrm{B}}}, \tag{2.16}$$

where $\Gamma_{\mathrm{B}} = (\Gamma_1 + \Gamma_2)/2$. We choose the barotropic vortex turnaround time to be of unit duration, $T_{\mathrm{B}} = 1$, and use this as the temporal basis for nondimensionalization.

In these units, the baroclinicity parameter, Γ, a measure for the difference in scale between coherent structures in the upper and lower layers, is simply measured by the ratio of circulations:

$$\Gamma = \frac{\Gamma_1 - \Gamma_2}{\Gamma_1 + \Gamma_2}. \tag{2.17}$$

The upper and lower layer circulations can therefore be written as

$$\begin{aligned} \Gamma_1 &= \Gamma_B(1+\Gamma), \\ \Gamma_2 &= \Gamma_B(1-\Gamma), \end{aligned} \tag{2.18}$$

which shows that the parameter Γ quantifies the deviation from purely barotropic flow. For the theory developed in the present paper, it is necessary that the potential vorticity in the upper and lower layer is single-signed, i.e., positive, so that Γ lies within the range $[-1, 1]$. The flow is purely barotropic, with equal potential vorticity in both layers, for $\Gamma = 0$ and is completely imbalanced, with vanishing potential vorticity in either the upper or lower layer for the extreme values, $\Gamma = \pm 1$.

3. Point-Vortex Equilibrium Statistical Mechanics

Evolving two-dimensional ideal flow is commonly observed to exhibit very different behavior at the largest and smallest scales of the vorticity field. As the flow evolves, the gradient of the vorticity field grows without bound, generating vorticity undulations on arbitrarily fine length scales. However, organization appears at the largest scales in the mean vorticity field as large-scale structures emerge from the turbulent interactions. These two qualitatively different patterns of behavior – random fluctuations on the smallest scales, coherent organization on the largest scales – are united within the theory of equilibrium statistical fluid mechanics. In effect, this theory predicts that the mean vorticity field that emerges at long times, subject to constraints on a few large-scale quantities such as energy and circulation, is precisely the one that is consistent with the greatest randomness in the smallest scales.

The key instrument of the equilibrium statistical theory is a nonlinear elliptic equation, called the *mean-field equation*, whose solution yields the mean stream function of the statistically most probable state of the fluid. To derive the equation for the mean field, however, it is necessary to parametrize the distribution of vorticity in the smallest scales. The use of the vortex model, in which regions of fluid vorticity are approximated by a point vortex, follows from the pioneering work of Onsager (1949), who restricted his study to the statistical behavior of finite collections of point vortices in a bounded domain. He demonstrated the existence of a critical energy, above which the point vortices condense into coherent structures. An extension of this idea to infinite collections of point vortices, each of identical strength, was carried out by Montgomery and Joyce (1974), who derived a closed equation for the mean-field stream function. A rigorous derivation of the mean-field equation based on a limiting sequence of Gibbs measures for collections of point vortices was later carried out by Caglioti *et al.* (1992) and Kiessling (1993), whose methods are adopted here.

In this paper we extend the equilibrium statistical model to a two-layer, quasigeostrophic fluid in all of space, a procedure that is described in detail in the Appendix. The point-vortex ensemble is distributed among both layers, with each point vortex of identical strength, ω_1, in the upper layer and a possibly different strength, ω_2, in the lower layer. The point-vortex ensemble conserves the pseudoenergy, the circulation in both layers, and, due to the rotational symmetry of the infinite domain, the angular momentum in the flow, all of which are defined in (2.10). For finite collections of point vortices we can easily construct a Gibbs measure, which yields a pair of equations that measure the probability of finding a point vortex in any given location. The Gibbs measure introduces two Lagrange multipliers, θ, which is associated with the energy constraint, and α, which is associated with the angular momentum constraint. The equations are valid, i.e., the sequence of Gibbs measures are properly normalized with $Z(N) < \infty$ in (A.8) provided that the Lagrange multipliers for energy and angular momentum, θ and α, respectively, satisfy the following constraints:

1. $\theta(N/4\pi) > -2$: at sufficiently high "inverse negative temperature" the solution collapses to a point vortex. Here utilizing standard terminology from statistical physics, the Lagrange multiplier for energy θ, has been identified with "inverse temperature". This quantity is not the physical temperature.
2. $\alpha, \omega_1, \omega_2 > 0$: the potential circulation, ω_1, ω_2, in the small-scale fields defined by the point vortices are of the same sign everywhere in the upper and lower layers with a Lagrange multiplier $\alpha > 0$. Otherwise, there are sets of positive measure of exact solutions involving clusters of oppositely signed point vortices that will pair up and propagate to arbitrarily distant locations and destroy the equilibrium statistical theory (Lim and Majda, 2000)

The angular momentum constraint in the infinite plane is therefore crucial in order to confine the mean-field potential vorticity within a localized region (Caglioti *et al.*, 1992; Eyink and Spohn, 1993) for even a finite-dimensional system of baroclinic vortices.

In the continuum limit of an infinite collection of point vortices, we derive an equation for the mean-field potential vorticity in each layer, which yields the average "density" of point vortices at any location in the domain.

Mean-Field Equations.

$$\begin{aligned} q_1 &\equiv \Delta\psi_1 - F(\psi_1 - \psi_2) = \Gamma_B(1+\Gamma)\frac{e^{(\theta\psi_1(\boldsymbol{x})-\alpha|\boldsymbol{x}|^2)\,\omega_1}}{\int e^{(\theta\psi_1(\boldsymbol{x})-\alpha|\boldsymbol{x}|^2)\,\omega_1}\,d\boldsymbol{x}}, \\ q_2 &\equiv \Delta\psi_2 + F(\psi_1 - \psi_2) = \Gamma_B(1-\Gamma)\frac{e^{(\theta\psi_2(\boldsymbol{x})-\alpha|\boldsymbol{x}|^2)\,\omega_2}}{\int e^{(\theta\psi_2(\boldsymbol{x})-\alpha|\boldsymbol{x}|^2)\,\omega_2}\,d\boldsymbol{x}}, \end{aligned} \tag{3.1}$$

where the constants θ and α are Lagrange multipliers whose values are determined by the pseudoenergy and angular momentum in the flow. The Lagrange multiplier θ is scaled by N, the number of point vortices in the flow. As discussed in the Appendix (see (A.17)–(A.19) below), the probability distribution for the density of point vortices in the mean-field limit, $N \to \infty$, is given in each layer by

$$\frac{e^{(\theta\psi_j(\boldsymbol{x})-\alpha|\boldsymbol{x}|^2)\omega_j}}{\int e^{(\theta\psi_j(\boldsymbol{x})-\alpha|\boldsymbol{x}|^2)\omega_j}\,d\boldsymbol{x}} \qquad \text{for} \quad j = 1, 2. \tag{3.2}$$

Since the left-hand side of the equations in (3.1) in the continuum limit $N \to \infty$ take the form of a weighted probability distribution, the circulation constraints are automatically satisfied. It has been shown in the barotropic case that all solutions to the mean-field equations are radially symmetric (Chanillo and Kiessling, 1995); the numerical experiments presented later in this paper strongly suggest that the addition of a baroclinic component does not break the radial symmetry in the regimes considered here. The solution of the mean-field equations in (3.1) can also be expressed through an empirical maximum entropy principle which is developed below (A.22) in the Appendix. This formulation leads to a numerical method for solving the mean-field equations in (3.1), based on the iterative algorithm given in Turkington and Whitaker (1996), and is described in Section 4.3.

4. Basic Solutions of Mean-Field Equations at "Zero Inverse Temperature"

The most probable mean state of the potential vorticity fields, q_1 and q_2, for a well-mixed, unbounded, two-layer quasigeostrophic fluid constrained by pseudoenergy, angular momentum, and circulations, solves the mean-field equations in (3.1). In general, these equations are nonlinear; however, in the special limit $\theta = 0$, known as the limit of "zero inverse temperature" due to the analogy between θ and $1/\beta$ in standard thermodynamics, the mean-field equations become linear in the stream functions ψ_1 and ψ_2 and can be solved exactly,

$$\begin{aligned} q_1 &\equiv \Delta\psi_1 - F(\psi_1 - \psi_2) = \Gamma_B(1+\Gamma)\frac{e^{-\alpha\omega_1|\boldsymbol{x}|^2}}{\int e^{-\alpha\omega_1|\boldsymbol{x}|^2}}, \\ q_2 &\equiv \Delta\psi_2 + F(\psi_1 - \psi_2) = \Gamma_B(1-\Gamma)\frac{e^{-\alpha\omega_2|\boldsymbol{x}|^2}}{\int e^{-\alpha\omega_2|\boldsymbol{x}|^2}}. \end{aligned} \tag{4.1}$$

At zero inverse temperature the most probable distributions of potential vorticity take on Gaussian profiles, whose extent is determined by the values of angular momentum and circulation alone.

In fact, at zero inverse temperature the energy constraint is removed entirely from consideration in calculating the most probable state of the fluid. The solution to the linear mean-field equations in (4.1) is the "most random" distribution of potential vorticity that has prescribed angular momentum and upper- and lower-layer

circulations but ranges over all possible energies. Qualitatively, these special solutions possess the key traits of the general case, such as confinement of the potential vorticity about the origin and barotropic far-field behavior of the stream function, yet have the virtue of mathematical tractability. By careful examination of the Gaussian zero inverse temperature solutions, we can trace which features of the flow are due to barotropic or baroclinic influences. Moreover, we can use these solutions as a benchmark in developing a numerical algorithm, based on the iterative method introduced by Turkington and Whitaker (1996), that solves the nonlinear mean-field equations in (3.1). Finally, the zero temperature states are excellent elementary prototype models for ocean sites that are preconditioned for convective overturning, a point that is further pursued in Section 5.1.

4.1. Purely Barotropic Flow

We begin with the purely barotropic case, $\Gamma = 0$, in which there is no vertical variation in the flow, and we establish properties of the most probable states in the infinite domain that are unaffected by baroclinic effects. First we show that these states are *localized* in space, unlike the zero inverse temperature states in an arbitrary, bounded domain. In bounded flow – where the angular momentum does not constrain the flow – the most random arrangement of potential vorticity is a uniform, flat distribution, with no structure in the mean. Here, on the infinite plane, the most random distribution of potential vorticity, given a definite angular momentum and circulation, is a Gaussian distribution with standard deviation, $\sigma = L_A$.

The nondimensionalized angular momentum for the potential vorticity profile in (4.1) is given by

$$\begin{aligned} A &= \sum_{j=1}^{2} \int_{\mathcal{R}^2} |\boldsymbol{x}|^2 \, \Gamma_{\mathrm{B}} \frac{\mathrm{e}^{-\alpha\omega_j |\boldsymbol{x}|^2}}{\int \mathrm{e}^{-\alpha\omega_j |\boldsymbol{x}|^2}} \\ &= \frac{2\Gamma_{\mathrm{B}}}{\alpha\omega}, \end{aligned} \tag{4.2}$$

where $\omega_1 = \omega_2 = \omega$ in purely barotropic flow. This can be rearranged to yield

$$\alpha\omega = \frac{2\Gamma_{\mathrm{B}}}{A} = \frac{1}{L_A^2}, \tag{4.3}$$

so that the mean-field equations in (4.1) reduce to

$$q_{\mathrm{B}} \equiv \Delta\psi_{\mathrm{B}} = \frac{\Gamma_{\mathrm{B}}}{\pi L_A^2} \, \mathrm{e}^{-(|\boldsymbol{x}|/L_A)^2}, \tag{4.4}$$

where $q_1 = q_2 = q_{\mathrm{B}}$. Therefore, the barotropic potential vorticity, q_{B} in (4.4), takes on a Gaussian profile with a standard deviation, σ, determined by the angular momentum, i.e.,

$$\sigma = \frac{1}{\sqrt{\alpha\omega}} = L_A. \tag{4.5}$$

The exact mean-field barotropic stream function, ψ_{B}, and velocity field, u_{B}, can be gained by integrating the potential vorticity, q_{B}, against the barotropic Green's function, G_{B}, (2.7),

$$\psi_{\mathrm{B}}(\boldsymbol{y}) = \int_{\mathcal{R}^2} \frac{1}{2\pi} \ln|\boldsymbol{x} - \boldsymbol{y}| \cdot \frac{\Gamma_{\mathrm{B}}}{\pi L_A^2} \, \mathrm{e}^{-(|\boldsymbol{x}|/L_A)^2} \mathrm{d}\boldsymbol{x}. \tag{4.6}$$

The integral is symmetric about the origin and can be evaluated in closed form to yield

$$\psi_{\mathrm{B}}(r) = \frac{\Gamma_{\mathrm{B}}}{2\pi} \left[\ln r + \tfrac{1}{2} \mathrm{Ei}\left(\frac{r^2}{L_A^2} \right) \right], \tag{4.7}$$

where r is the distance from the origin and $\mathrm{Ei}(x)$ is the exponential integral, defined as

$$\mathrm{Ei}(x) = \int_x^{\infty} \frac{\mathrm{e}^{-s}}{s} \, \mathrm{d}s. \tag{4.8}$$

Finally, the magnitude of the velocity field induced by a barotropic flow at zero inverse temperature is given as

$$|\boldsymbol{u}| \equiv \frac{\partial \psi_{\mathrm{B}}}{\partial r} = \frac{\Gamma_{\mathrm{B}}}{2\pi r}\left(1 - \tfrac{1}{2}\mathrm{e}^{-(r/L_A)^2}\right). \tag{4.9}$$

The barotropic stream function, ψ_{B}, is comprised of two distinct terms: (1) a long-range logarithmic term and (2) a short-range exponential integral term that drops off quickly at distances greater than L_A. At large distances, $r \gg L_A$, the far-field stream function asymptotically approaches a field induced by a point vortex with strength Γ_{B} concentrated at the origin. The exponential integral diverges at the origin, just enough to kill off the logarithmic singularity, and vanishes at distances greater than L_A. We show below in Section 4.2 that the asymptotic behavior of the far-field stream function is logarithmic even for flow with a nonzero baroclinic part, in which $\Gamma \neq 0$.

In Figure 1 we show the mean potential vorticity, q_{B} in part (a), the mean stream function, ψ_{B} in part (b), and the velocity field, $|\boldsymbol{u}|$ in part (c), for a purely barotropic flow at zero inverse temperature and a unit length, $L_A = 1$, which is the only length scale for a purely barotropic flow. In Figure 1(b), we have also plotted the logarithmic portion of the stream function; this gives a sense of how quickly the stream function approaches a "far-field" approximated by a point vortex of strength Γ_{B} placed at the origin. The length scale L_A governs each of the quantities plotted in Figure 1: (1) most of the potential vorticity is confined to a radius of distance L_A from the origin; (2) the stream function approaches the far-field value at approximately this length; and (3) the maximum velocity in the flow is achieved at a radius roughly L_A, forming a rim current.

4.2. Baroclinic Flow at Zero Inverse Temperature

Barotropic flow at zero inverse temperature is parametrized by a single length scale, L_A; the addition of a baroclinic component to the flow, however, adds two additional parameters to the problem: (1) the baroclinicity parameter, Γ, that measures the proportion of the potential vorticity difference between the upper and lower layers, and (2) the deformation radius, L_ρ, the length of typical undulations along the interface separating the two layers. As discussed earlier in Sections 2.1 and 2.3, we set the deformation radius to unity, $L_\rho = 1$, and test the effect of variations in baroclinicity and vortex radius. We concentrate on the parameter regime where $L_A \gg L_\rho$, which is most interesting for oceanographic phenomena.

The spread of the upper and lower vortices, which are equal in extent in the barotropic case, widen and contract in response to an increase in the baroclinicity in the flow. The potential vorticity of both layers at zero inverse temperature, which lie on the right-hand side of the mean-field equations in (3.1), take the form of a Gaussian distribution:

$$\begin{aligned} q_1 &= \frac{\Gamma_{\mathrm{B}}(1+\Gamma)^2}{\pi L_A^2}\,\mathrm{e}^{-(1+\Gamma)r^2/L_A^2} \\ q_2 &= \frac{\Gamma_{\mathrm{B}}(1-\Gamma)^2}{\pi L_A^2}\,\mathrm{e}^{-(1-\Gamma)r^2/L_A^2}. \end{aligned} \tag{4.10}$$

The standard deviation of the upper and lower layers are given by

$$\begin{aligned} \sigma_1 &= \frac{1}{\sqrt{\alpha\omega_1}} = \frac{L_A}{\sqrt{1+\Gamma}}, \\ \sigma_2 &= \frac{1}{\sqrt{\alpha\omega_2}} = \frac{L_A}{\sqrt{1-\Gamma}}. \end{aligned} \tag{4.11}$$

Thus, as Γ approaches the extreme values ± 1, the vortex in the upper (lower) layer is stronger and more compact, while the vortex in the lower (upper) layer weakens and spreads its potential vorticity over circles of larger radii. Due to the scalings of the upper- and lower-layer vortices in (4.11), it is clear that the spread of both the barotropic *and* baroclinic portions of the potential vorticity field are governed by the length scale, L_A.

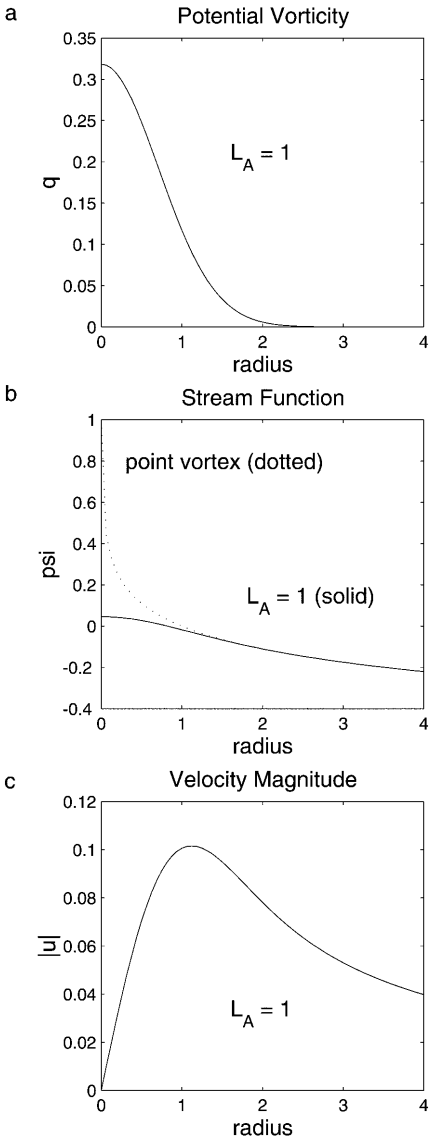

Figure 1. Barotropic flow at zero inverse temperature

Since the mean-field equations at zero inverse temperature in (4.10) are linear with respect to the upper- and lower-layer stream functions, we can easily invert and solve the equations numerically. In Figure 2 we show the potential vorticity fields and the stream functions for the zero inverse temperature states defined by a range of baroclinicity ratios, Γ, and barotropic vortex radii, L_A. Even for flow with a significant baroclinic component, the barotropic portion of the stream function quickly approaches the far-field logarithmic profile (Figure 2(a),(c)); the baroclinic portion of the stream function, however, drops to zero at distances beyond $(L_A + L_\rho)$ (Figure 2(b),(d)).

In Figure 2(a) we show how altering the proportion of circulation in the upper and lower layers – without changing the total amount of circulation in the flow or the length scale L_A – affects the barotropic component of the stream function. The barotropic field deviates only slightly from the asymptotic logarithmic profile at distances beyond unit lengths, for a range of solutions that range from the purely barotropic ($\Gamma = 0$) to the extreme case in which the baroclinic component accounts for half of the flow ($\Gamma = 1$). In Figure 2(c) we show that the asymptotic approach to a logarithmic profile, which is drawn with a dotted line, scales with the barotropic vortex radius, L_A. Here, $\Gamma = \frac{1}{2}$, so that the upper-layer vortex is three times stronger than the lower-layer vortex.

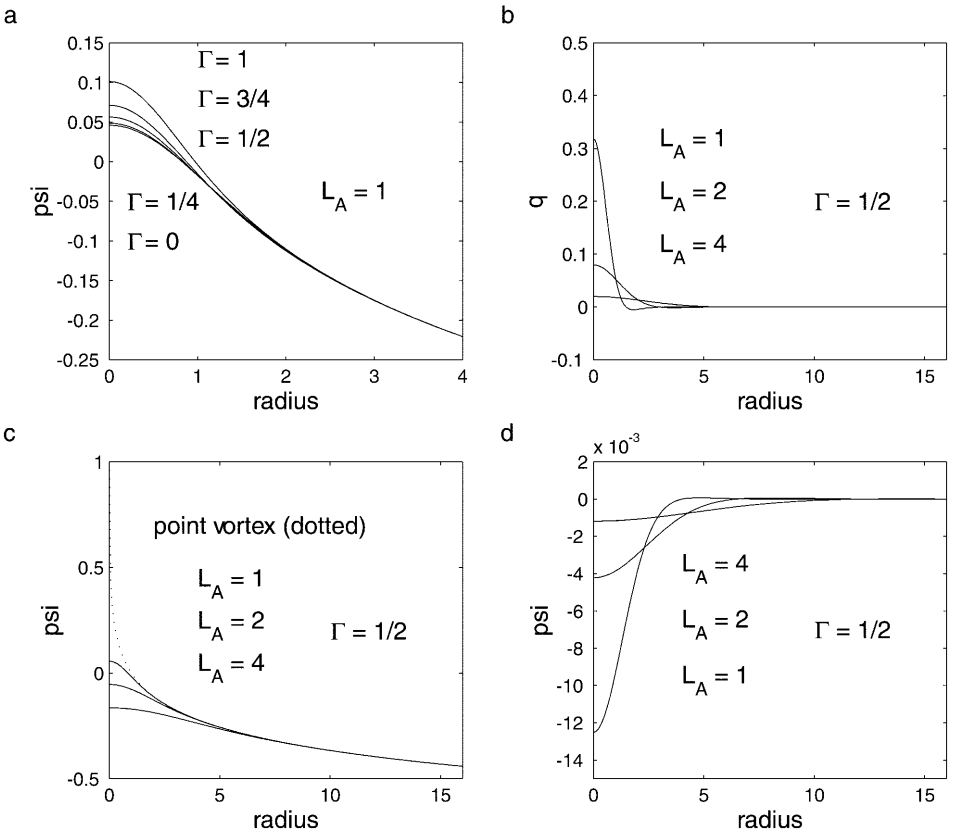

Figure 2. (a),(c) Barotropic stream function; (b),(d) baroclinic vorticity and stream function

In Figure 2(b),(d) we show that the spread of the baroclinic potential vorticity and stream fields is roughly measured by the sum of the length scales $(L_A + L_\rho)$. It is clear that the baroclinic portion of the potential vorticity field scales with the length scale L_A, since the spread of both the upper- and lower-layer vortices, which is given in (4.11), each scale with L_A. This is demonstrated in Figure 2(b) for the range L_A =1, 2, 4 at fixed baroclinicity, $\Gamma = \frac{1}{2}$. At larger values of L_A the radius of the baroclinic portion of the potential vorticity field spreads; the magnitude decreases since the total circulation in the flow is held constant. From the form of Green's function, G_T in (2.8), which vanishes at distances much greater than L_ρ, the baroclinic field cannot exert much influence beyond the deformation radius. Since the baroclinic field is demarcated by the length L_A, the baroclinic stream field must essentially vanish at distances larger than $(L_A + L_\rho)$. This is shown in Figure 2(d), in which the spread of the baroclinic portion of the stream function increases in the range L_A =1, 2, 4 at fixed baroclinicity, $\Gamma = \frac{1}{2}$, and falls rapidly to zero at distances greater than a deformation radius beyond the edge of the baroclinic vortex.

4.3. Numerical Algorithm

Numerical solution of the mean-field equations in (3.1) is based on the iterative algorithm developed by Turkington and Whitaker (1996), modified for the unbounded plane to account for the boundary conditions of vanishing flow at infinity. The algorithm, which is based on a maximum-entropy principle (see the Appendix for a derivation of the mean-field equations in (3.1) that follows from maximizing Shannon entropy (Jaynes, 1957)), replaces the quadratic energy functional with an convergent series of linear approximants. The resulting mean potential vorticity, which maximizes entropy and solves the mean-field equations, is produced as the energy converges upon the target value. Since the novel aspect of the algorithm in the current paper concerns the extension to the infinite plane, we concentrate on describing this aspect of the numerical procedure.

The difficulty lies in replacing the boundary conditions at infinity, where the flow must vanish, with an approximate condition on the stream function at a large, but finite, distance. We accomplish this by exploiting the asymptotic behavior of the barotropic and baroclinic components of the stream function, which are known exactly for solutions at zero inverse temperature. Due to the short range of influence of the baroclinic field, the far-field behavior of the stream function, at distances greater than $L_A + L_\rho$, is dominated by the barotropic component. In short, we can approximately solve the mean-field equations on an unbounded domain by executing the iterative algorithm on a finite domain of sufficiently large extent, supplemented by boundary conditions on the stream function that match the far-field barotropic field to leading order.

For solution of the mean-field equations at nonzero inverse temperatures, $\theta \neq 0$, this procedure depends on two crucial conditions:

1. the far-field stream function remains approximately barotropic;
2. the far-field potential vorticity field is dominated by the zero inverse temperature state, i.e., $\theta = 0$.

In fact, these two conditions remain true, provided that the length of the computational domain is sufficiently large.

Since the baroclinic stream function falls to zero at distances greater than L_ρ, we can ignore its contribution to the far-field stream function at large distances. The solution of the barotropic component of the problem can be approximated on a mesh as the sum of two parts:

$$\Delta\psi = f\,, \qquad f = \begin{cases} f_{\text{grid}}, & r < R, \quad (4.12) \\ f_{\text{far-field}}, & r > R, \quad (4.13) \end{cases}$$

where the distance, R, is sufficiently great so that $f_{\text{grid}} \approx f_{\text{far-field}}$.

We can therefore split the stream function into two parts, $\psi = \psi_{\text{far-field}} + \psi_{\text{remainder}}$, where the "far-field" stream function is known exactly and is valid through all of space:

$$\Delta\psi_{\text{far-field}} = f_{\text{far-field}} \qquad \text{(defined on all of space)} \tag{4.14}$$

and the remainder is defined on the grid,

$$\Delta\psi_{\text{remainder}} = f_{\text{grid}} - f_{\text{far-field}} \qquad \text{(defined on the grid)} \tag{4.15}$$

and $\psi_{\text{remainder}}$ vanishes on the grid boundaries.

At zero inverse temperature the far-field behavior of the barotropic stream function is known exactly, since

$$f_{\text{far-field}} = \frac{\Gamma_{\text{B}}}{\pi L_A^2}\left[(1+\Gamma)^2\,\mathrm{e}^{-(1+\Gamma)\,r^2/L_A^2} + (1-\Gamma)^2\,\mathrm{e}^{-(1-\Gamma)r^2/L_A^2}\right], \tag{4.16}$$

$$\psi_{\text{far-field}} = -\frac{1}{4\pi}\,\ln(r) - \frac{(1+\Gamma)}{8\pi}\,\mathrm{Ei}\left(\frac{(1+\Gamma)\,r^2}{L_A^2}\right) + \frac{(1-\Gamma)}{8\pi}\,\mathrm{Ei}\left(\frac{(1-\Gamma)\,r^2}{L_A^2}\right). \tag{4.17}$$

We utilize this explicit solution as the leading-order far-field solution for nonzero values of the inverse temperature, θ, with the same angular momentum and circulation. All that remains is to solve the remainder problem with Dirichlet boundary conditions, which is achieved numerically with the available elliptic solvers on a finite domain.

How good is this algorithm? The success of this method depends on the accuracy of the boundary conditions for the remainder stream function, $\psi_{\text{remainder}}$. At zero inverse temperature, $\theta = 0$, the remainder stream function is exactly zero. At larger (negative) values of the inverse temperature, the potential vorticity field is

$$f(\boldsymbol{x}) = \frac{\Gamma_1}{2}\,\frac{\mathrm{e}^{(\theta\psi_1 - \alpha|\boldsymbol{x}|^2)\,\omega_1}}{\int \mathrm{e}^{(\theta\psi_1 - \alpha|\boldsymbol{x}|^2)\,\omega_1}\,\mathrm{d}\boldsymbol{x}} + \frac{\Gamma_2}{2}\,\frac{\mathrm{e}^{(\theta\psi_2 - \alpha|\boldsymbol{x}|^2)\,\omega_2}}{\int \mathrm{e}^{(\theta\psi_2 - \alpha|\boldsymbol{x}|^2)\,\omega_2}\,\mathrm{d}\boldsymbol{x}}. \tag{4.18}$$

At large distances the far-field behavior of both the upper- and lower-layer stream functions, ψ_1 and ψ_2, is approximately barotropic,

$$\psi_1 = \psi_{\mathrm{B}} + \psi_{\mathrm{T}} \approx \psi_{\mathrm{B}} \sim -\frac{\Gamma_{\mathrm{B}}}{2\pi} \ln(r), \tag{4.19}$$

$$\psi_2 = \psi_{\mathrm{B}} - \psi_{\mathrm{T}} \approx \psi_{\mathrm{B}} \sim -\frac{\Gamma_{\mathrm{B}}}{2\pi} \ln(r), \tag{4.20}$$

where we have used the condition that $\Gamma_1 + \Gamma_2 = 2\Gamma_{\mathrm{B}}$. This leads to a far-field potential vorticity field with the form

$$f(\boldsymbol{x}) = \frac{\Gamma_1}{2} \frac{\mathrm{e}^{((\theta/4\pi)\,\ln(r) - \alpha r^2)\,\omega_1}}{\int \mathrm{e}^{((\theta/4\pi)\,\ln(r) - \alpha r^2)\,\omega_1}\,\mathrm{d}A} + \frac{\Gamma_2}{2} \frac{\mathrm{e}^{((\theta/4\pi)\,\ln(r) - \alpha r^2)\,\omega_2}}{\int \mathrm{e}^{((\theta/4\pi)\,\ln(r) - \alpha r^2)\,\omega_2}\,\mathrm{d}A}. \tag{4.21}$$

The approximation given above is good provided that

$$\alpha r^2 \gg \frac{\theta}{4\pi} \ln(r). \tag{4.22}$$

In practice, we have used the numerical algorithm with excellent results on finite domains whose extent is at least $4(L_A + L_\rho)$. The grid point resolution is no smaller than four points per unit length, so that the falloff in the baroclinic field is sufficiently resolved. We have calculated extensive numbers of solutions on numerous numerical grids of larger and smaller sizes and at greater and lesser resolutions and have found these numerical parameters are more than adequate to capture accurately the most probable states of the equilibrium statistical theory.

4.4. High-Energy Solutions

At very high energies and low angular momenta, the support of solutions to the mean-field equations in (3.1) is constricted about the origin while the peak potential vorticity in the flow may grow without bound. In general, the value of the inverse-temperature parameter, θ, affects the profile of the most probable state: for positive θ the profile is less steep than Gaussian, while for negative θ the profile is more steep than Gaussian. In short, the most probable state at high energy and strongly negative inverse temperature approaches a single point vortex located at the origin. This behavior is similar to that for the barotropic case (Caglioti *et al.*, 1992).

In Figure 3 we compare the potential vorticity of two barotropic solutions to the mean-field equations in (3.1), one at zero inverse temperature and one at high energy. Both solutions share identical angular momentum and total circulation in the flow. The potential vorticity field in Figure 3(a), in which the inverse temperature vanishes, has a Gaussian profile; the field in Figure 3(b), in which the temperature is strongly negative, is much steeper than Gaussian and is tightly restricted to a small radius about the origin. This implies, naturally, that the breadth of the vortex is affected by the energy as well as the angular momentum. The regime of intense strong vortices at high energies has correspondingly large velocities on the order of tens of meters per second dimensionally. The applications that are discussed next involve oceanographic flows with mean currents on the order of 10–15 cm/s dimensionally. In these low-energy regimes, the dependence of length scale of solutions on variation in energy is not significant. We model the preconditioned convection sites and open-ocean convection, discussed in Sections 5 and 6 below, by the zero inverse temperature states – and nearby states with low energy – as an illustrative model of the equilibrium statistical theory, so that the spread of the most probable states is well-estimated by the length scale, L_A.

5. Point-Vortex Models for Open-Ocean Convection

The ocean supports deep convection in just a few remote parts of the globe, including the Labrador Sea and the Greenland Sea in the North Atlantic, the Weddell Sea in the Antarctic, and the Mediterranean Sea (Marshall and Schott, 1999). It is an important wintertime phenomenon that helps to maintain the thermohaline

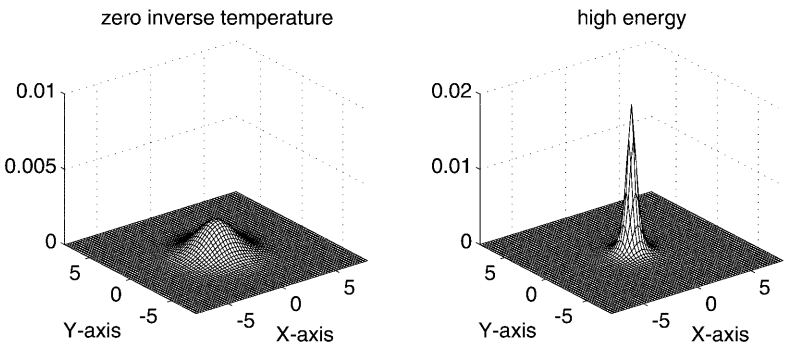

Figure 3. Barotropic potential vorticity at low and high energies

circulation and drive the poleward transfer of heat in the ocean. Open-ocean convection is induced by an extreme difference in temperature between cold air aloft and relatively warm ocean waters below, which cools the ocean surface and renders it less buoyant. On short time scales – within a day or so – the localized response to broad surface cooling is the formation of a collection of baroclinic "convective towers," each confined within a deformation radius, scattered across the domain. In a two-layer quasigeostrophic fluid, an individual convective tower can be modeled as a "heton" (Hogg and Stommel, 1985), a perfectly baroclinic arrangement of point vortices that is cyclonic in the upper layer and anticyclonic in the lower layer (Legg and Marshall, 1993).

DiBattista and Majda (1999a, 2000) and DiBattista *et al.* (2000) describe an equilibrium statistical model for convective overturning throughout a bounded domain, which captures the effects of strong cold-air outbreak that cools the surface homogeneously across the basin. In contrast, the quasigeostrophic model described below in Section 5.1 evolves in an *unbounded* domain. This is a natural choice for surface cooling that is *localized* in space. Here, to illustrate the theory, the preconditioned sites are modeled by zero inverse temperature states of the point-vortex equilibrium statistical theory, which produces a predominantly barotropic gyre confined within a radius, $r = L_A$, that is determined by the angular momentum in the flow. Convective overturning is modeled by a "cloud" of point-vortex hetons distributed within the gyre and parametrized by the change in baroclinicity in the flow.

5.1. Parametrization of Convective Overturning in the Point-Vortex Equilibrium Statistical Theory

A point-vortex heton (Hogg and Stommel, 1985) models the geostrophically balanced response, at short time scales of a day or so, to the convective mixing that results from buoyancy loss due to surface cooling (Legg and Marshall, 1993, 1998; Legg *et al.*, 1996). The convective mixing yields an exchange of fluid over a deformation radius between the warmer upper layer and the colder lower layer, which raises surfaces of constant density in the ocean interior. This generates a baroclinic vortical flow, cyclonic in the upper reaches of the ocean and anticyclonic below. In a two-layer fluid, a single convective tower, modeled by just a single heton, is parametrized by a potential vorticity anomaly, $\Delta\omega$: in the small area bound by the convective tower, the local potential vorticity is raised by the amount $\Delta\omega$ in the upper layer and is decreased by the amount $-\Delta\omega$ in the lower layer.

Recent numerical heton studies have simulated localized surface cooling by seeding hetons at random points within a circular region, preconditioned by quiescent initial flow (Legg and Marshall, 1993) and by barotropic cyclonic gyres (Legg and Marshall, 1998). In those studies, the preexisting gyre is induced by circular patches of constant potential vorticity; we capture the main dynamical features of the preconditioned flow – the local confinement of potential vorticity and the circumscribing barotropic rim current – with the zero inverse temperature states of the equilibrium statistical theory. These states, which were introduced in Section 4, possess a Gaussian distribution of potential vorticity, whose lateral extent is given by the length parameter, L_A. The central core of potential vorticity is surrounded by a barotropic rim current. In addition, we are free to add a nonvanishing baroclinic component to the preconditioned flow, which is parametrized by the baroclinicity parameter, Γ.

How do we incorporate localized convective overturning into the equilibrium statistical theory? We take advantage of the "point-vortex" nature of the heton, and alter the strengths of the point vortices, ω_1 and ω_2, that model the small-scale potential vorticity field in both the upper and lower layers:

$$\omega_1 \to \omega_1 + \Delta\omega, \tag{5.1}$$

$$\omega_2 \to \omega_2 - \Delta\omega. \tag{5.2}$$

The mean-field potential vorticity produced by the equilibrium statistical theory, which is observed on large scales, can be interpreted as the average "density" of point vortices in a small region of the flow (see (3.2) and the derivation provided in the Appendix). Convective overturning is modeled statistically for the general point-vortex configuration in (A.1) by adding a heton to each point vortex that contributes to the preexisting gyre, which increases the strength of the point vortex in the upper layer and decreases the strength in the lower layer. The distribution of hetons, which results from surface cooling, is confined within the radius, $r = L_A$.

The hetons are therefore distributed across the domain in exactly the same fashion as the preconditioned flow. Since each heton is purely baroclinic, the angular momentum cannot change. However, the total circulation due to the ensemble of hetons increases in the upper layer and decreases by a matching amount in the lower layer, an effect that simply changes the baroclinicity in the large-scale flow. Thus, we can parametrize convective overturning by a single parameter, $\Delta\Gamma$, so that the upper- and lower-layer circulations are given by

$$\begin{aligned} \Gamma_1 &= \Gamma_B(1 + \Gamma + \Delta\Gamma), \\ \Gamma_2 &= \Gamma_B(1 - \Gamma - \Delta\Gamma). \end{aligned} \tag{5.3}$$

Naturally, the energy is also changed by the addition of a heton ensemble; we delay this discussion to Section 6.

We must take care to ensure that the strength of convective overturning does not alter the sign of the circulations, Γ_1 and Γ_2 in (5.3). Should this occur, the equilibrium statistical theory, as developed in the Appendix, has no finite-dimensional Gibbs ensembles and can produce no most probable state. For an initial quiescent flow an ensemble of hetons immediately produces circulations of opposite sign in the upper and lower layers. In Legg and Marshall (1993) clusters of hetons form vortex pairs that propagate away from the cooling site. In support of these results there is rigorous mathematical evidence that a set of positive measure in phase space has solutions that escape to infinity (Lim and Majda, 2000). Here, we interpret the failure of the equilibrium statistical theory as an indication that the most probable arrangement of potential vorticity cannot be confined within any finite radius.

5.2. The Preconditioned Cyclonic Flows

The zero inverse temperature states described in Section 4, both the purely barotropic states and those with significant baroclinic components, are used to model preconditioned gyres subject to localized surface cooling. These are simple convenient cyclonic gyres with prototypical structure that depends on the angular momentum as established in Section 4. In laboratory and numerical experiments with localized surface cooling and actual observations in the Gulf of Lions (Legg and Marshall, 1998; Marshall and Schott, 1999) the preconditioned gyre and the region of localized cooling are both larger than the Rossby deformation radius. Thus, the radius of the preexisting gyre is fixed to be six times as large as the deformation radius, i.e., $L_A = 6L_\rho$. To test the effects of baroclinicity in the preconditioned flow we introduce five such examples with the baroclinicity parameter ranging from $\Gamma = 0, \pm\frac{1}{5}, \pm\frac{1}{2}$. The upper-layer flow is stronger than the lower-layer flow for positive values of Γ, and vice versa for negative values of Γ. The flow is purely barotropic for vanishing Γ; at the extreme value, $\Gamma = \frac{1}{2}$, the upper-layer flow is three times as strong as the lower-layer flow. Each of these solutions shown below in Figures 4 and 5 is used in Section 6 as a preconditioned gyre that supports convective overturning.

In Figure 4 we show the barotropic and baroclinic components of the preconditioned potential vorticity fields for $\Gamma = 0$, $\frac{1}{5}$, and $\frac{1}{2}$. Notice that the radius of both the barotropic and baroclinic vortices, whose scales

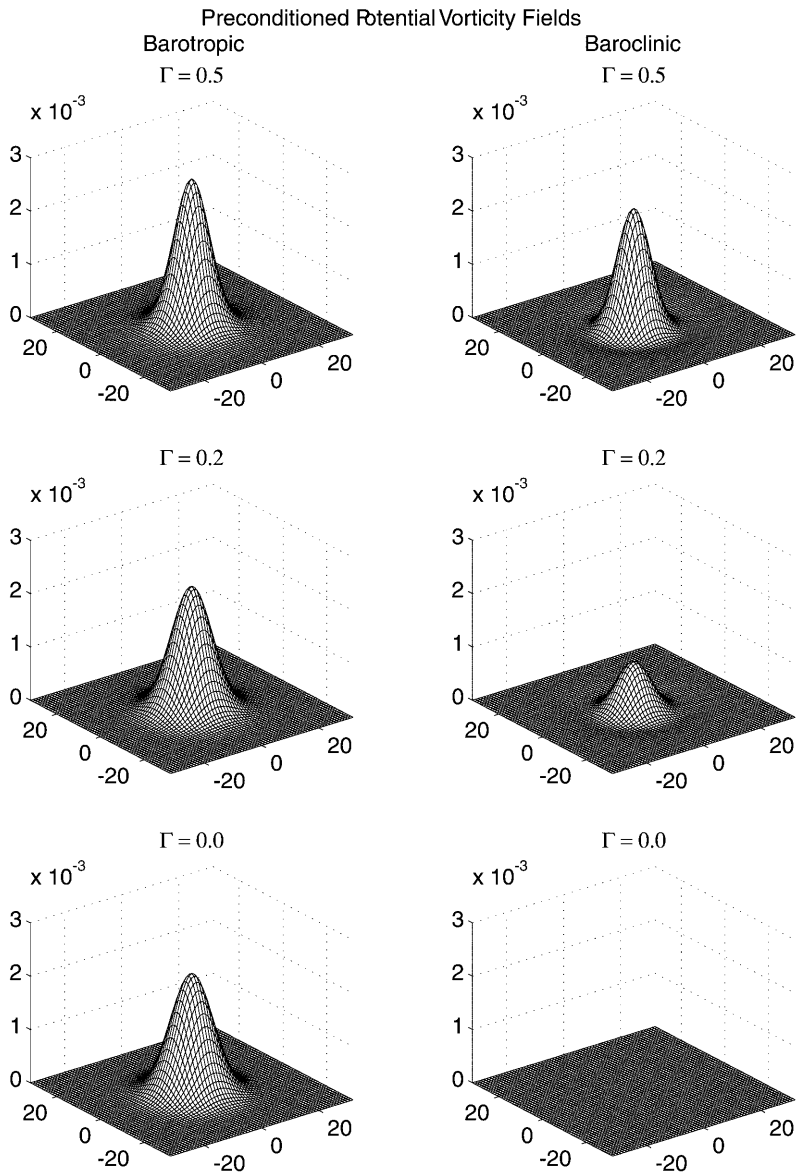

Figure 4

are set by L_A, does not appreciably change over this range of Γ. The baroclinic potential vorticity field, which measures the difference in magnitudes between the upper- and lower-layer flow, naturally vanishes for $\Gamma = 0$. For negative values of $\Gamma = -\frac{1}{5}$ and $-\frac{1}{2}$, the potential vorticity surfaces of the barotropic field are identical to corresponding examples shown in Figure 4; however, the baroclinic fields are inverted so that the potential vorticity surfaces are depressed. The magnitude of the baroclinic portion of the flow grows with increasing baroclinicity parameter.

The preconditioned thermal fields, which measure the deviation of the interface separating the two layers, are shown in Figure 5 for $\Gamma = 0$, $\frac{1}{5}$, and $\frac{1}{2}$. Here, like the baroclinic potential vorticity field, the interface is inverted for negative values of $\Gamma = -\frac{1}{5}$ and $-\frac{1}{2}$, so that the interface is depressed by stronger flow in the lower layer. The position of the interface, and the sign of the preconditioned temperature field, is directly related to the baroclinicity in the flow. The interface is raised for positive Γ, in which the upper-layer vortex is more powerful than the lower-layer vortex, flat for vanishing Γ, in which the upper- and lower-layer vortices are equal in strength, and is lower for negative Γ, in which the lower-layer vortex is more powerful than the upper-layer vortex. The width of the preconditioned thermal fields is approximately L_A in all cases shown.

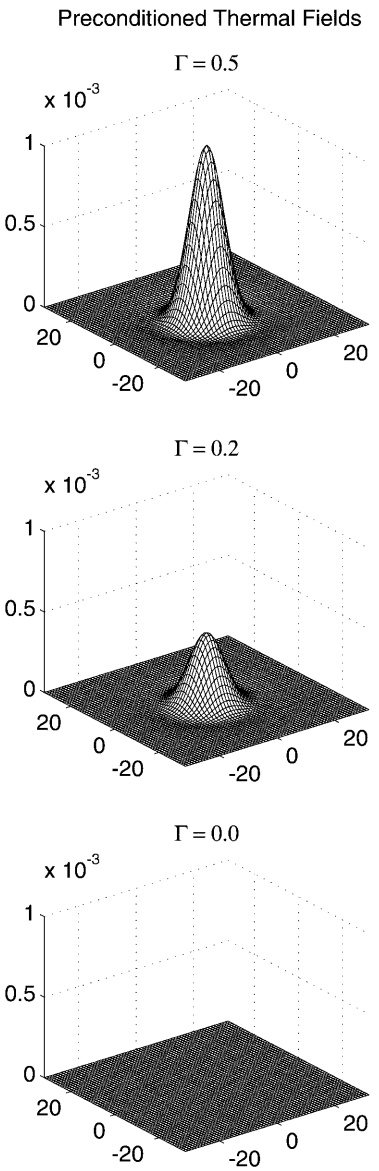

Figure 5

The solutions presented in Figures 4 and 5 are normalized by the length and time scales introduced in Section 2.3, i.e., by a unit deformation radius and unit turnaround time in the barotropic vortex. It is a simple matter to change the scale to fit the physical scales that typically govern convection in the ocean. When carrying out a dimensional analysis we usually scale the deformation radius to be approximately 10 km so that the radius of the preconditioned gyre is 60 km. The circulation in the barotropic field is adjusted so that the barotropic rim current has a maximum velocity of approximately 15 cm/s, typical values for oceanographic currents (Pedlosky, 1979).

6. Predictions for Convective Overturning Within Preconditioned Gyres

We have described a point-vortex equilibrium statistical theory tailored to the phenomenon of open-ocean convection in Section 5. In particular, as an illustration, the states with zero inverse temperature are used to model preexisting, predominantly barotropic gyres. The preconditioned sites are parametrized by two con-

stants: (1) a typical length scale, $L_A \gg L_\rho$, which is greater than the deformation radius, and (2) a parameter that measures the baroclinic portion of the flow, Γ, which tends to be positive.

Suppose these preconditioned gyres are subject to a localized cooling event. According to our discussion in Section 5.1, the effects of convective overturning are captured in the statistical theory by an additional parameter $\Delta\Gamma > 0$, which adds circulation to the upper layer and removes circulation in the lower layer. Convective overturning also introduces some additional energy into the fluid. Therefore, we parametrize the convective forcing with a pair, $(\Delta\Gamma, \Delta E)$. The value of additional energy is chosen so that the strongest heton ensemble that we consider, $\Delta\Gamma = 0.1$, strengthens the magnitude of velocity in the barotropic flow by approximately 15%, which in dimensional terms increases from 15 cm/s to approximately 17.5 cm/s. For weaker episodes of convective forcing, we scale the energy quadratically with respect to the induced circulation, which leads to a linear change in velocity magnitude. In all the examples that we have calculated – for both purely barotropic gyres and for preconditioning with a significant baroclinic part – the potential vorticity and cold-temperature anomalies introduced by surface cooling are contained within the radius, $r = L_A$. The spread of these quantities in the gyre is more compact for stronger upper-layer flow ($\Gamma > 0$) and more spread for stronger lower-layer flow ($\Gamma < 0$).

In Figures 6 and 7 we show the potential vorticity anomalies, both barotropic and baroclinic components, and the temperature anomalies introduced by heton ensembles parametrized by $\Delta\Gamma = 0.01, 0.05$, and 0.1. The energy, ΔE, is chosen so that the maximum velocity scales linearly with the strength of the heton ensemble. The preconditioned flow is purely barotropic. The lateral extent of both the potential vorticity and temperature anomalies is limited by the length scale, L_A, even for the weakest case. The magnitude of the induced anomalies, however, scales with the increasing strength of the surface forcing.

In Figures 8 and 9 we show the potential vorticity anomalies, both barotropic and baroclinic components, and the temperature anomalies introduced by heton ensembles parametrized by $\Delta\Gamma = 0.1$. Here, the preconditioned flow is given for a range of $\Gamma = 0, \pm\frac{1}{5}$, and $\pm\frac{1}{2}$, which are shown in Figures 4 and 5. The purely barotropic preconditioned state is represented in the middle row; above lie states in which the upper-layer flow is stronger and below lie states in which the lower-layer flow is stronger. A number of trends are evident in these diagrams: (1) the barotropic and baroclinic potential vorticity anomalies and the temperature anomalies are confined within a radius, $r = L_A$; (2) the baroclinic potential vorticity and the temperature anomalies are most constricted for states in which the upper-layer flow is strongest and most relaxed for states in which the lower-layer flow is strongest; (3) the barotropic potential vorticity anomaly is broadest for the preconditioned purely barotropic gyre.

In all of the examples in Figures 8 and 9, it is evident from the sign of the potential vorticity anomalies that the velocity field due to the heton ensemble from convective overturning always strengthens the preexisting cyclonic gyre. The influence of the heton ensemble does not quite reach the barotropic rim current, however, because the radius of maximum velocity increase lies within the radius, $r = L_A$. The results in Figures 8 and 9 yield statistical predictions that the conclusions gained from the heton studies by Legg and Marshall (1993, 1998) – that the barotropic governor confines potential vorticity and cold-temperature anomalies and suppresses baroclinic instability – should hold even for preconditioned gyres that contain baroclinic components. The only requirement is that the strength of the heton ensemble not be sufficiently large to change the sign of the circulation in the lower layer. The steady states produced by the statistical theory have potential vorticity of the same sign in each layer and are stable according to the Charney–Stern criterion (Pedlosky, 1979). Thus, the predicted steady states from the statistical theory predict a stable long time response.

7. Conclusions

We have developed a point-vortex equilibrium statistical model for open-ocean convection within the context of a two-layer quasigeostrophic fluid in an unbounded domain. We use the statistical theory to produce both the cyclonic, largely barotropic gyres that model preconditioned convection sites and the small-scale convective towers, approximated by point-vortex hetons, that form in response to strong localized surface cooling. Due to the constraint on the angular momentum in the flow, which follows from the rotational symmetry of the unbounded domain, the potential vorticity of the most probable states is confined within a length, L_A in (2.14), about the origin. Convective overturning is parametrized in the statistical theory by a change in

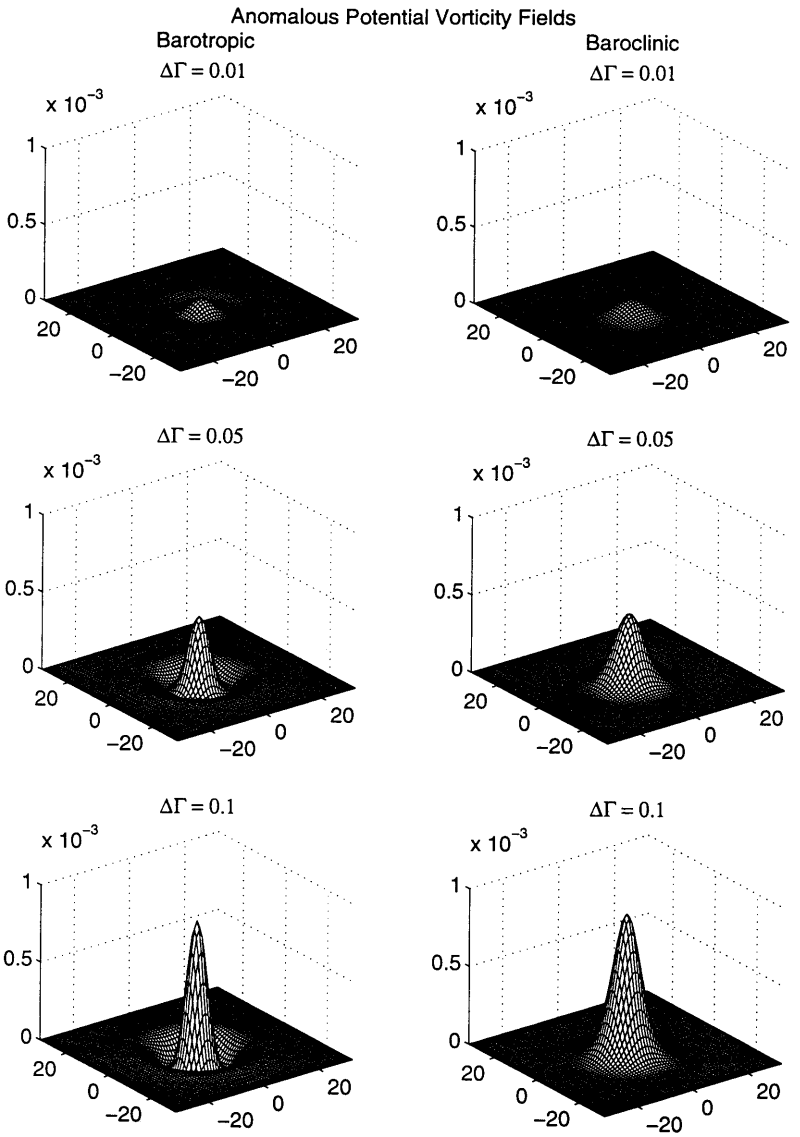

Figure 6

baroclinicity, $\Delta\Gamma$, in the large-scale flow. Thus, we have developed a model for surface cooling that is *localized* above the preexisting gyre. The most probable state of a localized episode of strong surface cooling is produced as the solution to the mean-field equations in (3.1), after specifying the strengths of both the preconditioned gyre and the convective overturning.

Recent numerical heton studies have simulated localized surface cooling by seeding baroclinic point vortex pairs at random points within a circular region at uniform intervals of time. The preexisting flow within the localized convection site can drastically affect the long-term distribution of hetons. Hetons seeded within an initially quiescent flow quickly establish a baroclinic rim current that is susceptible to baroclinic instabilities – clusters of oppositely signed hetons form vortex pairs between the two layers that propagate away from the cooled region (Legg and Marshall, 1993). However, a disk preconditioned by cyclonic, barotropic, and uniform potential vorticity has been shown to suppress baroclinic instability, so that the potential vorticity anomalies and cold-temperature anomalies due to convective overturning are confined within the gyre (Legg and Marshall, 1998).

The equilibrium statistical theory predicts – without resolution of the detailed dynamics – that baroclinic instability is always suppressed in this manner, provided that the convective overturning is not so severe as

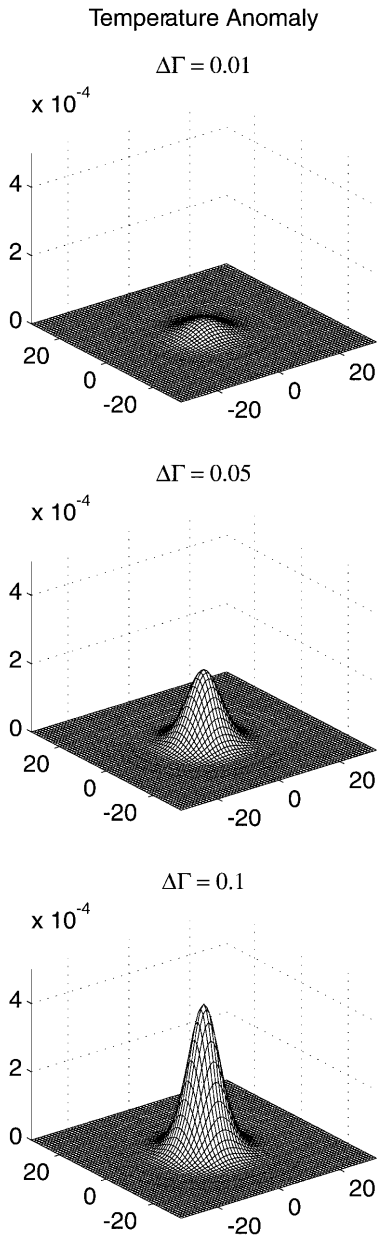

Figure 7

to change the sign of the circulation in the lower layer. For surface cooling over an initially quiescent flow, however, the equilibrium statistical model in the present paper is poorly defined, and the angular momentum constraint cannot be satisfied by any solution to the mean-field equations. We interpret this to mean that oppositely signed clusters of vorticity can always pair up and propagate to arbitrarily distant points in the domain (Lim and Majda, 2000).

For simplicity here, prototypical preconditioned gyres are modeled within the equilibrium statistical theory as zero inverse temperature states, simple exact Gaussian solutions to the mean-field equations at special energies as discussed in Section 4. The potential vorticity of these states are confined within a radius, $r = L_A$, governed by a barotropic rim current that reaches its maximum at this distance. Heton ensembles – the products of strong surface buoyancy forcing – are parametrized by a single value, $\Delta\Gamma$, that measure the increase in upper-layer circulation and the decrease in lower-layer circulation that follows widespread convective overturning. The distribution of hetons matches the concentration of potential vorticity in the preexisting

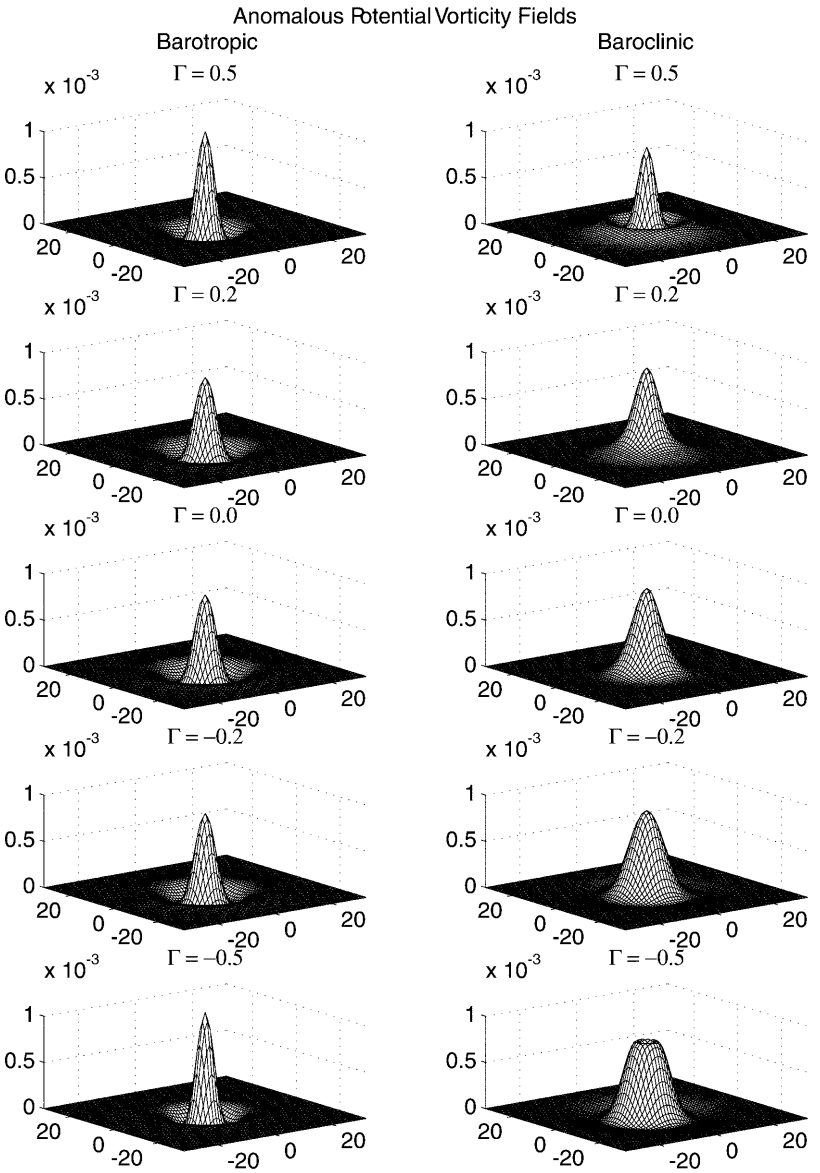

Figure 8

gyre; thus, surface cooling is localized in space. We find that potential vorticity and cold-temperature anomalies, which are the products of convective overturning, are always confined within the radius, $r = L_A$, and governed by the barotropic rim current, provided that the lower-layer circulation remains positive. This conclusion holds, even for preconditioned gyres that contain a significant baroclinic component of the flow. All of these conclusions point to the possibility of using equilibrium statistical solutions to parametrize ocean convection without resolving it in detail. It is a very interesting issue to confirm the role of the angular momentum constraint predicted here with direct simulations.

Appendix. Derivation of Two-Layer Mean-Field Equation in All of Space

The most probable distribution of the mean potential vorticity of a two-dimensional fluid at equilibrium is formally given by a Gibbs measure. In a two-layer quasigeostrophic model – constrained by pseudoenergy, angular momentum, and circulations in the upper and lower layer – the statistically most probable state is

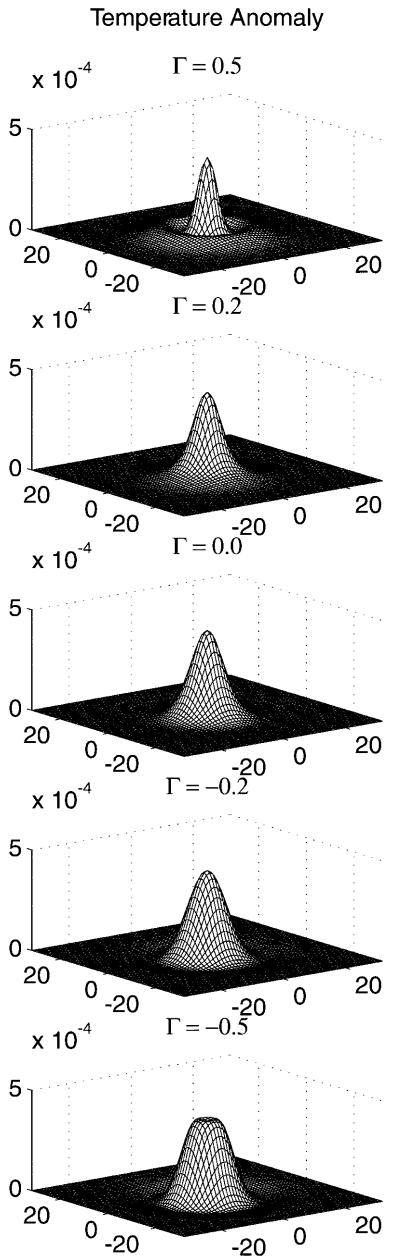

Figure 9

given by the coupled mean-field equations in (3.1), which relates the Gibbs measures for the mean potential vorticity in the upper and lower layers to the mean stream functions.

However, in order to derive the mean-field equations for a continuous field, for which the phase space is infinite-dimensional and the phase volume ill-defined, it is necessary first to construct a series of finite-dimensional approximations, each with finite-dimensional phase space, whose limit is well-defined. Here, the continuous potential vorticity field is approximated by large collections of point vortices of constant strength within each layer. We construct a series of Gibbs measures for a fluid composed of point vortices, and take the limit, with the appropriate scalings for the constrained quantities, as the number of point vortices diverges.

To begin, we introduce N point vortices in a quiescent initial flow at random locations $\boldsymbol{x}_{1i}$ in the upper layer and $\boldsymbol{x}_{2m}$ and lower layer, $1 \leq i, m \leq N$, so that the potential vorticity is given by

$$\begin{aligned} q_1^{(N)} &= \sum_{i=1}^{N} \omega_1 \delta_{\boldsymbol{x}_{1i}}, \\ q_2^{(N)} &= \sum_{m=1}^{N} \omega_2 \delta_{\boldsymbol{x}_{2m}}. \end{aligned} \tag{A.1}$$

The collection of point vortices induces flow in both the upper and lower layers, whose stream functions, $\psi_1^{(N)}$ and $\psi_2^{(N)}$, are

$$\begin{aligned} \psi_1^{(N)}(\boldsymbol{x}) &= \frac{\omega_1}{2} \sum_{j=1}^{N} \left[G_{\mathrm{B}}(\boldsymbol{x}, \boldsymbol{x}_j) + G_{\mathrm{T}}(\boldsymbol{x}, \boldsymbol{x}_j) \right] + \frac{\omega_2}{2} \sum_{n=1}^{N} \left[G_{\mathrm{B}}(\boldsymbol{x}, \boldsymbol{x}_n) - G_{\mathrm{T}}(\boldsymbol{x}, \boldsymbol{x}_n) \right], \\ \psi_2^{(N)}(\boldsymbol{x}) &= \frac{\omega_1}{2} \sum_{j=1}^{N} \left[G_{\mathrm{B}}(\boldsymbol{x}, \boldsymbol{x}_j) - G_{\mathrm{T}}(\boldsymbol{x}, \boldsymbol{x}_j) \right] + \frac{\omega_2}{2} \sum_{n=1}^{N} \left[G_{\mathrm{B}}(\boldsymbol{x}, \boldsymbol{x}_n) + G_{\mathrm{T}}(\boldsymbol{x}, \boldsymbol{x}_n) \right], \end{aligned} \tag{A.2}$$

where G_{B} and G_{T} are Green's functions, defined in (2.7) and (2.8), that govern the barotropic and the baroclinic components of the flow. In (A.2), the summation index of j denotes upper-layer point vortices from (A.1) with strength ω_1, while the index n is used for the lower-layer vortices with strength ω_2.

Two-dimensional flow on the infinite plane inherits conserved quantities related to invariances of the dynamics and domain including energy, H, center of vorticity, $\boldsymbol{M}$, and angular momentum, A, which are given by the

Conserved Quantities.

$$\begin{aligned} H &= -\frac{1}{2} \int \psi_1 q_1 - \frac{1}{2} \int \psi_2 q_2, \\ \boldsymbol{M} &= \int \boldsymbol{x}_1 q_1 + \int \boldsymbol{x}_2 q_2, \\ A &= \int \boldsymbol{x}_1^2 q_1 + \int \boldsymbol{x}_2^2 q_2, \end{aligned} \tag{A.3}$$

as well as the circulation in each layer:

$$\begin{aligned} \Gamma_1 &= \int q_1, \\ \Gamma_2 &= \int q_2. \end{aligned} \tag{A.4}$$

As a finite-dimensional Hamiltonian system, the point-vortex system has the following conserved quantities (Hogg and Stommel, 1985), which are discrete analogues of those in (A.3):

$$\begin{aligned} H^{(N)} &= -\frac{\omega_1^2}{4} \sum_{i=1}^{N} \sum_{j=1}^{N} \left[G_{\mathrm{B}}(\boldsymbol{x}_i, \boldsymbol{x}_j) + G_{\mathrm{T}}(\boldsymbol{x}_i, \boldsymbol{x}_j) \right] - \frac{\omega_1 \omega_2}{2} \sum_{i=1}^{N} \sum_{n=1}^{N} \left[G_{\mathrm{B}}(\boldsymbol{x}_i, \boldsymbol{x}_n) - G_{\mathrm{T}}(\boldsymbol{x}_i, \boldsymbol{x}_n) \right] \\ &\quad - \frac{\omega_2^2}{4} \sum_{m=1}^{N} \sum_{j=1}^{N} \left[G_{\mathrm{B}}(\boldsymbol{x}_m, \boldsymbol{x}_n) + G_{\mathrm{T}}(\boldsymbol{x}_m, \boldsymbol{x}_n) \right], \\ \boldsymbol{M}^{(N)} &= \omega_1 \sum_{i=1}^{N} \boldsymbol{x}_{1i} + \omega_2 \sum_{m=1}^{N} \boldsymbol{x}_{2m}, \\ A^{(N)} &= \omega_1 \sum_{i=1}^{N} \boldsymbol{x}_{1i}^2 + \omega_2 \sum_{m=1}^{N} \boldsymbol{x}_{2m}^2. \end{aligned} \tag{A.5}$$

There are additional constraints on the circulation in each layer, which amounts to the conservation of the number and strength of the point vortices:

$$\begin{aligned} \Gamma_1^{(N)} &= \omega_1 \sum_{i=1}^{N} 1 \equiv N\omega_1, \\ \Gamma_2^{(N)} &= \omega_2 \sum_{m=1}^{N} 1 \equiv N\omega_2. \end{aligned} \tag{A.6}$$

Notice that the energy functional does not account for the infinite self-energy associated with each point vortex. Also, the center of vorticity which is the conserved quantity associated with translational invariance, may be identified with the origin of the domain, $\boldsymbol{M} = 0$, with no loss of generality.

The Gibbs measure for the point-vortex ensemble, which is the probability measure that contains the least bias given the constraints in (A.5), is therefore defined by

$$\begin{aligned} \mathrm{d}\mu_N = {} & \frac{1}{Z(N)} \mathrm{e}^{\left(-\theta H^{(N)}(\boldsymbol{x}_{11},\ldots,\boldsymbol{x}_{1N},\boldsymbol{x}_{21},\ldots,\boldsymbol{x}_{2N}) - \alpha\left(\sum \omega_1 |x_{1i}|^2 + \sum \omega_2 |x_{2m}|^2\right) - \gamma_1\omega_1 N - \gamma_2\omega_2 N\right)} \\ & \cdot \mathrm{d}\boldsymbol{x}_{11} \cdots \mathrm{d}\boldsymbol{x}_{1N}\, \mathrm{d}\boldsymbol{x}_{21} \cdots \mathrm{d}\boldsymbol{x}_{2N}, \end{aligned} \tag{A.7}$$

where θ and α are the Lagrange multipliers associated with the given energy and angular momentum constraints and γ_1 and γ_2 are the Lagrange multipliers associated with the upper- and lower-layer circulation constraints. The partition function, $Z(N)$, is a normalizing quantity ensuring that $d\mu_N$ is a probability measure,

$$\begin{aligned} Z(N) = {} & \int \mathrm{e}^{\left(-\theta H^{(N)}(\boldsymbol{x}_{11},\ldots,\boldsymbol{x}_{1N},\boldsymbol{x}_{21},\ldots,\boldsymbol{x}_{2N}) - \alpha\left(\sum \omega_1 |x_{1i}|^2 + \sum \omega_2 |x_{2m}|^2\right) - \gamma_1\omega_1 N - \gamma_2\omega_2 N\right)} \\ & \cdot \mathrm{d}\boldsymbol{x}_{11} \cdots \mathrm{d}\boldsymbol{x}_{1N} \mathrm{d}\boldsymbol{x}_{21} \cdots \mathrm{d}\boldsymbol{x}_{2N}. \end{aligned} \tag{A.8}$$

A major concern is that the partition function remains finite throughout the sequence of Gibbs measures for the point-vortex ensembles so that a meaningful result is derived in the limit as $N \to \infty$. The exponential integrand can be expanded into a finite product of simpler elements, each of which must have finite weight. Expansion of the pseudoenergy, H, leads to products of the barotropic and baroclinic Green's functions, G_{B} and G_{T}. The baroclinic Green's function is short in range, essentially vanishing at distances greater than the deformation radius, L_ρ, with the same local singularity as the barotropic Green's function. The barotropic Green's function is logarithmic, $G_{\mathrm{B}}(\boldsymbol{x}, \boldsymbol{y}) = (1/2\pi) \ln |\boldsymbol{x} - \boldsymbol{y}|$, which leads to upper bounds on the energy locally in space involving products of the form

$$|\boldsymbol{x}|^{N\theta/4\pi}. \tag{A.9}$$

The extra factor of one-half in comparing Green's function singularity with the integrand in (A.8) arises because the Hamiltonian in (A.3) and (A.5) has an extra factor of one-half.

The angular momentum constraint contributes terms with the form

$$\begin{aligned} & \mathrm{e}^{-\alpha\omega_1 \sum |x_{1i}|^2} \\ & \mathrm{e}^{-\alpha\omega_2 \sum |x_{2m}|^2}, \end{aligned} \tag{A.10}$$

which decay rapidly at infinity provided that α, ω_1, and ω_2 all share the same sign and that $\alpha \neq 0$. With (A.9) and (A.10) the partition function $Z(N)$ is finite, $Z(N) < \infty$, provided that θ satisfies

$$\frac{N\theta}{4\pi} > -2. \tag{A.11}$$

Therefore the vorticity in both layers cannot be oppositely signed. This technical requirement prevents the formation of vortex pairs in opposite layers, which can propagate to arbitrarily far distances (Lim and Majda, 2000). In this paper the potential vorticity is positive so that all quantities are greater than zero, $\omega_1, \omega_2, \alpha > 0$.

Finally, we note the circulation constraints contribute only a constant factor to the numerator and denominator of the Gibbs measure. By the appropriate scaling of the Lagrange multipliers, γ_j, by γ_j/N, we can eliminate the circulation terms, since they do not affect the value of the probability measure as $N \to \infty$. Later, we show that the circulation constraint is automatically satisfied.

When we take the limit as $N \to \infty$, we need to take care that the Gibbs measure, $d\mu_N$, and the partition function, $Z(N)$, hold roughly steady and approach nontrivial distributions as the number of point vortices in the ensemble in (A.1) diverges. The form of the restriction on the Lagrange multiplier associated with the energy in (A.9), suggests that we replace θ by θ/N as we approach the limit as $N \to \infty$.

We can identify the probability density of single vortices in the upper and lower layers with the mean potential vorticity field in the continuum limit. For an arbitrary location, $\boldsymbol{x}$, this is expressed, for a large but finite collection of N vortices, as the pair of one-point probability functions

$$\rho_{1N}(\boldsymbol{x}) = \frac{\int \mathrm{e}^{-(\theta/N)H^{(N)}(\boldsymbol{x},\boldsymbol{x}_{11},\dots,\boldsymbol{x}_{1N-1},\boldsymbol{x}_{21},\dots,\boldsymbol{x}_{2N}) - \alpha(\omega_1|\boldsymbol{x}|^2 + \omega_1\sum|x_{1j}|^2 + \omega_2\sum|x_{2n}|^2)} \mathrm{d}\boldsymbol{x}_{11}\cdots\mathrm{d}\boldsymbol{x}_{1N-1}\mathrm{d}\boldsymbol{x}_{21}\cdots\mathrm{d}\boldsymbol{x}_{2N}}{Z(N)}, \tag{A.12}$$

$$\rho_{2N}(\boldsymbol{x}) = \frac{\int \mathrm{e}^{-(\theta/N)H^{(N)}(\boldsymbol{x},\boldsymbol{x}_{11},\dots,\boldsymbol{x}_{1N},\boldsymbol{x}_{21},\dots,\boldsymbol{x}_{2N-1}) - \alpha(\omega_1|\boldsymbol{x}|^2 + \omega_1\sum|x_{1j}|^2 + \omega_2\sum|x_{2n}|^2)} \mathrm{d}\boldsymbol{x}_{11}\cdots\mathrm{d}\boldsymbol{x}_{1N}\mathrm{d}\boldsymbol{x}_{21}\cdots\mathrm{d}\boldsymbol{x}_{2N-1}}{Z(N)}.$$

As the number of point vortices diverges, we make the tacit assumption in the formal derivation that the density of potential vorticity converges, in a weak sense, to the continuous probability functions

$$\begin{aligned} \frac{1}{N}\sum_{i=1}^{N}\omega_1\delta_{\boldsymbol{x}_{1i}} &\rightharpoonup \omega_1\rho_1(\boldsymbol{x}), \\ \frac{1}{N}\sum_{m=1}^{N}\omega_2\delta_{\boldsymbol{x}_{2m}} &\rightharpoonup \omega_2\rho_2(\boldsymbol{x}) \qquad \text{as} \quad N\to\infty. \end{aligned} \tag{A.13}$$

Thus, for functions defined on both upper and lower layers, $f = (f_1, f_2)$, we have

$$\sum_{i=1}^{N}\frac{\omega_1}{N}f_1(\boldsymbol{x}_{1i}) + \sum_{m=1}^{N}\frac{\omega_2}{N}f_2(\boldsymbol{x}_{2m}) \to \omega_1\int f_1(\boldsymbol{y})\,\rho_1(\boldsymbol{y})\,\mathrm{d}\boldsymbol{y} + \omega_2\int f_2(\boldsymbol{y})\,\rho_2(\boldsymbol{y})\,\mathrm{d}\boldsymbol{y}\,. \tag{A.14}$$

Now we simply expand the energy functional, $H^{(N)}$, to gain the energy at a location $\boldsymbol{x}$ occupied by an arbitrary point vortex, in terms of the ensemble spanned by $N-1$ point vortices, which yields

$$\begin{aligned} \frac{1}{N}H^{(N)}(\boldsymbol{x},\boldsymbol{x}_{11},\dots,\boldsymbol{x}_{1N-1},\boldsymbol{x}_{21},\dots,\boldsymbol{x}_{2N}) &= \frac{1}{N}H^{(N-1,N)}(\boldsymbol{x}_{11},\dots,\boldsymbol{x}_{1N-1},\boldsymbol{x}_{21},\dots,\boldsymbol{x}_{2N}) \\ &\quad -\frac{1}{N}\frac{\omega_1^2}{2}\sum_{j=1}^{N}\big[G_{\mathrm{B}}(\boldsymbol{x},\boldsymbol{x}_j)+G_{\mathrm{T}}(\boldsymbol{x},\boldsymbol{x}_j)\big] - \frac{1}{N}\frac{\omega_1\omega_2}{2}\sum_{n=1}^{N}\left[G_{\mathrm{B}}(\boldsymbol{x},\boldsymbol{x}_n)-G_{\mathrm{T}}(\boldsymbol{x},\boldsymbol{x}_n)\right], \end{aligned} \tag{A.15}$$

$$\begin{aligned} \frac{1}{N}H^{(N)}(\boldsymbol{x},\boldsymbol{x}_{11},\dots,\boldsymbol{x}_{1N},\boldsymbol{x}_{21},\dots,\boldsymbol{x}_{2N-1}) &= \frac{1}{N}H^{(N,N-1)}(\boldsymbol{x}_{11},\dots,\boldsymbol{x}_{1N},\boldsymbol{x}_{21},\dots,\boldsymbol{x}_{2N-1}) \\ &\quad -\frac{1}{N}\frac{\omega_1\omega_2}{2}\sum_{j=1}^{N}\big[G_{\mathrm{B}}(\boldsymbol{x},\boldsymbol{x}_j)-G_{\mathrm{T}}(\boldsymbol{x},\boldsymbol{x}_j)\big] - \frac{1}{N}\frac{\omega_2^2}{2}\sum_{n=1}^{N}\left[G_{\mathrm{B}}(\boldsymbol{x},\boldsymbol{x}_n)+G_{\mathrm{T}}(\boldsymbol{x},\boldsymbol{x}_n)\right]. \end{aligned} \tag{A.16}$$

Thus, with the tacit assumptions in (A.13) and (A.14), in the limit as $N \to \infty$, the explicit sums of the

equations are given by

$$
\begin{aligned}
&-\frac{1}{N}\frac{\omega_1^2}{2}\sum_{j=1}^{N}\big[G_{\mathrm{B}}(\boldsymbol{x},\boldsymbol{x}_j)+G_{\mathrm{T}}(\boldsymbol{x},\boldsymbol{x}_j)\big]-\frac{1}{N}\frac{\omega_1\omega_2}{2}\sum_{n=1}^{N}[G_{\mathrm{B}}(\boldsymbol{x},\boldsymbol{x}_n)-G_{\mathrm{T}}(\boldsymbol{x},\boldsymbol{x}_n)]\\
&\quad\to-\frac{\omega_1}{2}\int[G_{\mathrm{B}}(\boldsymbol{x},\boldsymbol{y})+G_{\mathrm{T}}(\boldsymbol{x},\boldsymbol{y})]\,\rho_1(\boldsymbol{y})\,\mathrm{d}\boldsymbol{y}-\frac{\omega_1}{2}\int[G_{\mathrm{B}}(\boldsymbol{x},\boldsymbol{y})-G_{\mathrm{T}}(\boldsymbol{x},\boldsymbol{y})]\,\rho_2(\boldsymbol{y})\,\mathrm{d}\boldsymbol{y},\\
&-\frac{1}{N}\frac{\omega_1\omega_2}{2}\sum_{j=1}^{N}\big[G_{\mathrm{B}}(\boldsymbol{x},\boldsymbol{x}_j)-G_{\mathrm{T}}(\boldsymbol{x},\boldsymbol{x}_j)\big]-\frac{1}{N}\frac{\omega_2^2}{2}\sum_{n=1}^{N}[G_{\mathrm{B}}(\boldsymbol{x},\boldsymbol{x}_n)+G_{\mathrm{T}}(\boldsymbol{x},\boldsymbol{x}_n)]\\
&\quad\to-\frac{\omega_2}{2}\int[G_{\mathrm{B}}(\boldsymbol{x},\boldsymbol{y})-G_{\mathrm{T}}(\boldsymbol{x},\boldsymbol{y})]\,\rho_1(\boldsymbol{y})\mathrm{d}\boldsymbol{y}-\frac{\omega_2}{2}\int[G_{\mathrm{B}}(\boldsymbol{x},\boldsymbol{y})+G_{\mathrm{T}}(\boldsymbol{x},\boldsymbol{y})]\,\rho_2(\boldsymbol{y})\mathrm{d}\boldsymbol{y},
\end{aligned}
$$

which are naturally related to the stream functions

$$
\begin{aligned}
\psi_1(\boldsymbol{x}) &= -\tfrac{\omega_1}{2}\textstyle\int[G_{\mathrm{B}}(\boldsymbol{x},\boldsymbol{y})+G_{\mathrm{T}}(\boldsymbol{x},\boldsymbol{y})]\,\rho_1(\boldsymbol{y})\mathrm{d}\boldsymbol{y}-\tfrac{\omega_2}{2}\int[G_{\mathrm{B}}(\boldsymbol{x},\boldsymbol{y})-G_{\mathrm{T}}(\boldsymbol{x},\boldsymbol{y})]\,\rho_2(\boldsymbol{y})\mathrm{d}\boldsymbol{y},\\
\psi_2(\boldsymbol{x}) &= -\tfrac{\omega_1}{2}\textstyle\int[G_{\mathrm{B}}(\boldsymbol{x},\boldsymbol{y})-G_{\mathrm{T}}(\boldsymbol{x},\boldsymbol{y})]\,\rho_1(\boldsymbol{y})\mathrm{d}\boldsymbol{y}-\tfrac{\omega_2}{2}\int[G_{\mathrm{B}}(\boldsymbol{x},\boldsymbol{y})+G_{\mathrm{T}}(\boldsymbol{x},\boldsymbol{y})]\,\rho_2(\boldsymbol{y})\mathrm{d}\boldsymbol{y}\ .
\end{aligned}
$$

Thus, in the continuum limit the one-point probability densities are given by

$$
\begin{aligned}
\rho_1(\boldsymbol{x}) &\approx \rho_{1N}(\boldsymbol{x}) \approx \frac{\mathrm{e}^{-\theta\omega_1\psi_1(\boldsymbol{x})-\alpha\omega_1|\boldsymbol{x}|^2}\,\widetilde{Z}(N-1,N)}{Z(N)},\\
\rho_2(\boldsymbol{x}) &\approx \rho_{2N}(\boldsymbol{x}) \approx \frac{\mathrm{e}^{-\theta\omega_2\psi_2(\boldsymbol{x})-\alpha\omega_2|\boldsymbol{x}|^2}\,\widetilde{Z}(N,N-1)}{Z(N)},
\end{aligned}
\tag{A.17}
$$

with

$$
\begin{aligned}
\widetilde{Z}(N-1,N) &= \int \mathrm{e}^{\left(-\theta H^{(N-1,N)}(\boldsymbol{x}_{11},\dots,\boldsymbol{x}_{1N-1},\boldsymbol{x}_{21},\dots,\boldsymbol{x}_{2N})-\alpha\left(\sum\omega_1|x_{1i}|^2+\sum\omega_2|x_{2m}|^2\right)-\gamma_1\omega_1N-\gamma_2\omega_2N\right)}\\
&\quad\cdot\mathrm{d}\boldsymbol{x}_{11}\cdots\mathrm{d}\boldsymbol{x}_{1N-1}\mathrm{d}\boldsymbol{x}_{21}\cdots\mathrm{d}\boldsymbol{x}_{2N},\\
\widetilde{Z}(N,N-1) &= \int \mathrm{e}^{\left(-\theta H^{(N,N-1)}(\boldsymbol{x}_{11},\dots,\boldsymbol{x}_{1N},\boldsymbol{x}_{21},\dots,\boldsymbol{x}_{2N-1})-\alpha\left(\sum\omega_1|x_{1i}|^2+\sum\omega_2|x_{2m}|^2\right)-\gamma_1\omega_1N-\gamma_2\omega_2N\right)}\\
&\quad\cdot\mathrm{d}\boldsymbol{x}_{11}\cdots\mathrm{d}\boldsymbol{x}_{1N}\mathrm{d}\boldsymbol{x}_{21}\cdots\mathrm{d}\boldsymbol{x}_{2N-1}\ .
\end{aligned}
\tag{A.18}
$$

Since ρ_1, ρ_{1N}, ρ_2, and ρ_{2N} are all probability densities we necessarily have the relations, as $N\to\infty$,

$$
\begin{aligned}
\frac{Z(N)}{\widetilde{Z}(N-1,N)} &\approx \int \mathrm{e}^{-\theta\omega_1\psi_1(\boldsymbol{x})-\alpha\omega_1|\boldsymbol{x}|^2}\mathrm{d}\boldsymbol{x},\\
\frac{Z(N)}{\widetilde{Z}(N,N-1)} &\approx \int \mathrm{e}^{-\theta\omega_2\psi_2(\boldsymbol{x})-\alpha\omega_2|\boldsymbol{x}|^2}\mathrm{d}\boldsymbol{x}.
\end{aligned}
\tag{A.19}
$$

Substitution of the ratio of partition functions in (A.19) back into the probability density functions in (A.17) yields the following

Mean-Field Equations.

$$
\begin{aligned}
q_1 &\equiv \Delta\psi_1 - F(\psi_1-\psi_2) = \Gamma_1\frac{\mathrm{e}^{(-\theta\psi_1(\boldsymbol{x})-\alpha|\boldsymbol{x}|^2)\omega_1}}{\int\mathrm{e}^{(-\theta\psi_1(\boldsymbol{x})-\alpha|\boldsymbol{x}|^2)\,\omega_1}\,\mathrm{d}\boldsymbol{x}},\\
q_2 &\equiv \Delta\psi_2 + F(\psi_1-\psi_2) = \Gamma_2\frac{\mathrm{e}^{(-\theta\psi_2(\boldsymbol{x})-\alpha|\boldsymbol{x}|^2)\omega_2}}{\int\mathrm{e}^{(-\theta\psi_2(\boldsymbol{x})-\alpha|\boldsymbol{x}|^2)\,\omega_2}\,\mathrm{d}\boldsymbol{x}},
\end{aligned}
\tag{A.20}
$$

where we have identified the mean-field potential vorticities, q_1 and q_2, with the one-point probability densities. Also, the multiplicative constant before the potential vorticity probability densities is expressed in terms of the nondimensionalized total circulations, Γ_1 and Γ_2, since

$$\begin{aligned} \Gamma_1 &= \int q_1, \\ \Gamma_2 &= \int q_2. \end{aligned} \tag{A.21}$$

This completes the formal derivation. There is no doubt that a generalization of the results in Caglioti *et al.* (1992) can be utilized to make these calculations rigorous.

An Empirical Maximum-Entropy Principle. There is an alternative derivation of the mean-field equations in (A.20) based on a maximum-entropy principle, which justifies the usage of the numerical algorithm – due to Turkington and Whitaker (1996) and discussed in Section 4.3 – that is used to construct the most probable states of the equilibrium statistical theory. The most probable state of the two-layer fluid at statistical equilibrium is postulated to maximize the information, or Shannon entropy, S, in the coarse-grained field (Jaynes, 1957) represented by the one-point probability distributions, $\rho_1(\boldsymbol{x}, \lambda)$ and $\rho_2(\boldsymbol{x}, \lambda)$,

$$S\left(\rho_1(\boldsymbol{x}, \lambda), \Pi_{01}(\lambda); \rho_2(\boldsymbol{x}, \lambda), \Pi_{02}(\lambda)\right) \equiv -\sum_{j=1}^{2} \iint \rho_j(\boldsymbol{x}, \lambda) \ln \frac{\rho_j(\boldsymbol{x}, \lambda)}{\Pi_{0j}(\lambda)} \, \mathrm{d}\lambda \, \mathrm{d}\boldsymbol{x}. \tag{A.22}$$

Here, the one-point probability distributions are functions of both space and the range of vorticity. The influence of the small-scale vorticity field is expressed through the prior distributions, $\Pi_{01}(\lambda)$ and $\Pi_{02}(\lambda)$, that appear in the entropy functional in (A.22). For the present case in which the small-scale vorticity field is made up of point vortices of identical strength ω_1 and ω_2 in each layer, we have

$$\begin{aligned} \Pi_{01} &= \delta_{\omega_1}(\lambda), \\ \Pi_{02} &= \delta_{\omega_2}(\lambda). \end{aligned} \tag{A.23}$$

For clarity of exposition, however, we provide a general derivation of the mean-field equations for arbitrary Π_{0j} and impose the point-vortex prior distributions in (A.23) only at the final step.

As described above the most probable state of the two-layer fluid is constrained by the pseudoenergy, H, angular momentum, A, and circulations, Γ_1 and Γ_2:

$$\begin{aligned} H(\rho_1, \rho_2) &= -\sum_{j=1}^{2} \int \tfrac{1}{2} \psi_j q_j \, \mathrm{d}\boldsymbol{x} = H_0, \\ A(\rho_1, \rho_2) &= \sum_{j=1}^{2} \int |\boldsymbol{x}_j|^2 q_j \, \mathrm{d}\boldsymbol{x} = A_0, \\ \Gamma_j(\rho_j) &= \int q_j \, \mathrm{d}\boldsymbol{x}_j = \Gamma_{0j}, \qquad j = 1, 2, \end{aligned} \tag{A.24}$$

which are expressed in terms of the mean-field potential vorticities,

$$\begin{aligned} q_1(\boldsymbol{x}) &= \int \lambda \rho_1(\boldsymbol{x}, \lambda) \, \mathrm{d}\lambda, \\ q_2(\boldsymbol{x}) &= \int \lambda \rho_2(\boldsymbol{x}, \lambda) \, \mathrm{d}\lambda. \end{aligned} \tag{A.25}$$

Furthermore, we add two additional formal constraints that ensure the one-point distributions, ρ_1 and ρ_2, are probability measures,

$$P_j = \iint \rho_j \, \mathrm{d}\lambda \, \mathrm{d}\boldsymbol{x} = 1, \qquad j = 1, 2. \tag{A.26}$$

The extremization of the Shannon entropy in (A.22) subject to the constraints listed in (A.24) and (A.26) is a straightforward exercise in the calculus of variations. We extremize the quantity

$$\begin{aligned} -S(\rho_1, \Pi_{01}; \rho_2, \Pi_{02}) + \theta\,(H(\rho_1, \rho_2) - H_0) + \alpha\,(A(\rho_1, \rho_2) - A_0) + \gamma_1(\Gamma_1(\rho_1) - \Gamma_{10}) \\ +\ \gamma_2(\Gamma_2(\rho_2) - \Gamma_{20}) + \tilde{\mu}_1(P_1(\rho_1) - 1) + \tilde{\mu}_2(P_2(\rho_2) - 1), \end{aligned} \tag{A.27}$$

where the values θ, α, and γ_j are the Lagrange multipliers associated with the energy, angular momentum, and circulation in each layer. The multipliers $\tilde{\mu}_j$ ensure that ρ_j satisfy the requirements of a probability measure.

By taking the first variation of (A.27) with respect to ρ_1 and ρ_2,

$$\begin{aligned} -\frac{\delta S}{\delta\rho_1} + \theta\frac{\delta E}{\delta\rho_1} + \alpha\frac{\delta A}{\delta\rho_1} + \gamma_1\frac{\delta\Gamma_1}{\delta\rho_1} + \tilde{\mu}_1\frac{\delta P_1}{\delta\rho_1} &= 0, \\ -\frac{\delta S}{\delta\rho_2} + \theta\frac{\delta E}{\delta\rho_2} + \alpha\frac{\delta A}{\delta\rho_2} + \gamma_2\frac{\delta\Gamma_2}{\delta\rho_2} + \tilde{\mu}_2\frac{\delta P_2}{\delta\rho_2} &= 0, \end{aligned} \tag{A.28}$$

and substituting the functional derivatives

$$\frac{\delta S}{\delta\rho_j} = -1 - \ln\left(\frac{\rho_j}{\Pi_{0j}}\right), \qquad \frac{\delta H}{\delta\rho_j} = -\psi_j\,\lambda\,, \qquad \frac{\delta A}{\delta\rho_j} = |\boldsymbol{x}_j|^2\lambda\,, \qquad \frac{\delta\Gamma_j}{\delta\rho} = \lambda\,, \qquad \frac{\delta P_j}{\delta\rho} = 1, \tag{A.29}$$

we have

$$\begin{aligned} \ln\left(\frac{\rho_1}{\Pi_{01}}\right) + 1 &= (\theta\psi - \alpha\boldsymbol{x} - \gamma_1)\lambda + \tilde{\mu}_1, \\ \ln\left(\frac{\rho_2}{\Pi_{02}}\right) + 1 &= (\theta\psi - \alpha\boldsymbol{x} - \gamma_2)\lambda + \tilde{\mu}_2. \end{aligned} \tag{A.30}$$

Applying the probability constraints in (A.26) yields, after rearrangement,

$$\begin{aligned} \rho_1 &= \frac{\mathrm{e}^{(\theta\psi_1 - \alpha|\boldsymbol{x}|^2 - \gamma_1)\lambda}\,\Pi_{01}(\lambda)}{\int \mathrm{e}^{(\theta\psi_1 - \alpha|\boldsymbol{x}|^2 - \gamma_1)\lambda}\,\Pi_{01}(\lambda)\,\mathrm{d}\lambda\,\mathrm{d}\boldsymbol{x}}, \\ \rho_2 &= \frac{\mathrm{e}^{(\theta\psi_2 - \alpha|\boldsymbol{x}|^2 - \gamma_2)\lambda}\,\Pi_{02}(\lambda)}{\int \mathrm{e}^{(\theta\psi_2 - \alpha|\boldsymbol{x}|^2 - \gamma_2)\lambda}\,\Pi_{02}(\lambda)\,\mathrm{d}\lambda\,\mathrm{d}\boldsymbol{x}}. \end{aligned} \tag{A.31}$$

Finally, substituting the point-vortex prior distributions, Π_{0j} in (A.23), enforcing the circulation constraints in (A.24) and integrating against the vorticity field yields the mean-field equations

$$\begin{aligned} q_1 \equiv \Delta\psi_1 - F(\psi_1 - \psi_2) &= \Gamma_1\frac{\mathrm{e}^{(\theta\psi_1(\boldsymbol{x}) - \alpha|\boldsymbol{x}|^2)\,\omega_1}}{\int \mathrm{e}^{(-\theta\psi_1(\boldsymbol{x}) - \alpha|\boldsymbol{x}|^2)\,\omega_1}\,\mathrm{d}\boldsymbol{x}}, \\ q_2 \equiv \Delta\psi_2 + F(\psi_1 - \psi_2) &= \Gamma_2\frac{\mathrm{e}^{(\theta\psi_2(\boldsymbol{x}) - \alpha|\boldsymbol{x}|^2)\,\omega_2}}{\int \mathrm{e}^{(-\theta\psi_2(\boldsymbol{x}) - \alpha|\boldsymbol{x}|^2)\,\omega_2}\,\mathrm{d}\boldsymbol{x}}, \end{aligned} \tag{A.32}$$

which are identical to those in (A.20).

References

Caglioti, E., Lions, P.L., Marchioro, C., and Pulvirenti, M. (1992). A special class of stationary flows for two-dimensional Euler equations: a statistical mechanics description. *Commun. Math. Phys.*, **143**, 501–525.

Carnevale, G., and Frederiksen, J. (1987). Nonlinear stability and statistical mechanics of flow over topography. *J. Fluid Mech.*, **175**, 157–181.

Chanillo, S., and Kiessling, M. (1995). Rotational symmetry of solutions of some nonlinear problems in statistical mechanics and in geometry. *Commun. Math. Phys.*, **160**, 217–238.

DiBattista, M.T., and Majda, A.J. (1999a). An equilibrium statistical model for the spreading phase of open-ocean convection. *Proc. Natl. Acad. Sci.*, **96**, 6009–6013.

DiBattista, M.T., and Majda, A.J. (1999b). Metastability of equilibrium statistical states for geophysical flows with damping and driving. Submitted to *Phys. D*.

DiBattista, M.T., and Majda, A.J. (2000). An equilibrium statistical theory for large-scale features of open-ocean convection. *J. Phys. Oceanogr.*, **30**, 1325–1353.

DiBattista, M.T., Majda, A.J., and Marshall, M. (2000). A statistical theory for the "patchiness" of open-ocean deep convection: the effect of preconditioning. Accepted and to appear in *J. Phys. Oceanogr.*

Eyink, G.L., and Spohn, H. (1993). Negative-temperature states and large-scale, long-lived vortices in two-dimensional turbulence. *J. Stat. Phys.*, **70**, 833–886.

Grote, M.J., and Majda, A.J. (1997). Crude closure dynamics through large-scale statistical theory. *Phys. Fluids*, **9**, 3431–3442.

Grote, M.J., and Majda, A.J. (2000). Crude closure for flow with topography through large scale statistical theory. *Nonlinearity*, **13**, 569–600.

Hogg, N.G., and Stommel, H.M. (1985). Hetonic explosions: the breakup and spread of warm pools as explained by baroclinic point vortices. *J. Atmos. Sci.*, **42**, 1465–1476.

James, I.N. (1987). Suppression of baroclinic instability in horizontally sheared flows. *J. Atmos. Sci.*, **44**, 3710–3720.

Jaynes, E.T. (1957). Information theory and statistical mechanics. *Phys. Rev.*, **106**, 620–630.

Kazantsev, E., Sommeria, J., and Verron, J. (1998). Subgrid-scale eddy parameterization by statistical mechanics in a barotropic ocean model. *J. Phys. Oceanogr.*, **28**, 1017–1042.

Kiessling, M.K.H. (1993). Statistical mechanics of classical particles with logarithmic interactions. *Commun. Pure Appl. Math.*, **46**, 27–56.

Legg, S., Jones, H. and Visbeck, M. (1996). A heton perspective of baroclinic eddy transfer in localized ocean deep convection. *J. Phys. Oceanogr.*, **26**, 2251–2266.

Legg, S., and Marshall, J. (1993). A heton model of the spreading phase of open-ocean deep convection. *J. Phys. Oceanogr.*, **23**, 1040–1056.

Legg, S., and Marshall, J. (1998). The influence of the ambient flow on the spreading of convective water masses. *J. Mar. Res.*, **56**, 107–139.

Lim, C.C., and Majda, A.J. (2000). Point vortex dynamics for coupled surface/interior QG and propagating heton clusters in models for ocean convection. Accepted and to appear in *Geophys. Astrophys. Fluid Dynamics*.

Majda, A.J., and Bertozzi, A. (2000). *Vorticity and the Mathematical Theory of Incompressible Flow*, Cambridge University Press, Cambridge.

Marshall, J., and Schott, F. (1999). Open-ocean convection: observations, theory and models. *Rev. Geophys.*, **37**, 1–64.

Miller, J., Weichman, P.B., and Cross, M.C. (1992). Statistical mechanics, Euler's equation, and Jupiter's Red Spot. *Phys. Rev. A*, **45**, 2328–2359.

Montgomery, D., and Joyce, G. (1974). Statistical mechanics of "negative temperature" states. *Phys. Fluids*, **17**, 1139–1145.

Onsager, L. (1949). Statistical hydrodynamics. *Nuovo Cimento Suppl.*, **6**, 297–287.

Pedlosky, J. (1979). *Geophysical Fluid Dynamics*. Springer-Verlag, New York.

Salmon, R., Holloway, G., and Hendershott, M.C. (1976). The equilibrium statistical mechanics of simple quasigeostrophic models. *J. Fluid Mech.*, **75**, 691–703.

Turkington, B., and Whitaker, N. (1996). Statistical equilibrium computations of coherent structures in turbulent shear layers. *SIAM J. Sci. Comput.*, **17**, 1414–1433.